CERN-SPSC-89-17
SPSC/M-440
March 6,1989

Memorandum to the SPSC Committee Proposing the Addition of a Downstream TPC to the NA35 Apparatus for the 1990 Data Taking Period

NA35 Collaboration

J. BARTKE[5], J. BÄCHLER[8], H. BIALKOWSKA[11], R. BOCK[6], R. BROCKMANN[6], M. CALICCHIO[2], S.I. CHASE[3], I. DERADO[10], V. ECKARDT[10], J. ESCHKE[7], C. FAVUZZI[2], D. FERENC[13], H. FESSLER[10], B. FLEISCHMAN[6], P. FREUND[10], M. FUCHS[6], M. GAZDZICKI[7], H.J. GEBAUER[10], E. GLADYSZ[5], J.W. HARRIS[3], E. HARTIG[7], W. HECK[7], M. HOFFMAN[8], K. KADIJA[13], A. KARABARBOUNIS[1], R. KEIDEL[9], M. KOWALSKI[5], M. LAHANAS[7], J.-Y. LEE[7], A. LJUBICIC JR.[13], S. MARGETIS[7], E. NAPPI[2], G. ODYNIEC[3], G. PAIC[13,6], A.D. PANAGIOTOU[4,1], A. PETRIDIS[1], J. PFENNIG[7], A. PIPER[9], F. POSA[2], H.G. PUGH[3], F. PÜHLHOFER[9], G. RAI[3], W. RAUCH[3], R. RENFORDT[7], D. RÖHRICH[7], H. ROTHARDT[7], K. RUNGE[8], A. SANDOVAL[6], I. SCHNEIDER[7], N. SCHMITZ[10], E. SCHMOETTEN[8], L.S. SCHROEDER[3], J. SEYBOTH[10], P. SEYBOTH[10], J. SEYERLEIN[10], E. SKRZYPCZAK[12], P. SPINELLI[2], R. STOCK[7], H. STRÖBELE[7], A. THOMAS[7], L. TEITELBAUM[3], S. TONSE[3], G. VASILEIADIS[1], G. VESZTERGOMBI[10,a], D. VRANIC[13], S. WENIG[7], M. WENSVEEN[6]

1) Physics Department, University of Athens 157-71 Athens, Greece
2) Dipartimento di Fisica, Universita di Bari, and INFN, I-70126 Bari, Italy
3) Lawrence Berkeley Laboratory, University of California, Berkeley CA 94720, USA
4) CERN, CH 1211 Geneva 23, Switzerland
5) Institute of Nuclear Physics, PL 30055 Cracow, Poland
6) Gesellschaft für Schwerionenforschung, D-6100 Darmstadt 11, Fed. Rep. Germany
7) Fachbereich Physik, Universität Frankfurt, D-6000 Frankfurt, Fed. Rep. Germany
8) Fakultät für Physik, Universität Freiburg, D-7800 Freiburg, Fed. Rep. Germany
9) Fachbereich Physik, Universität Marburg, D-3550 Marburg, Fed. Rep. Germany
10) Max-Planck-Institut für Physik und Astrophysik, D-8000 München 40, Fed. Rep. Germany
11) Institute of Nuclear Studies, PL-00681 Warsaw, Poland
12) Institute of Experimental Physics, Univ. of Warsaw, PL-00681 Warsaw, Poland
13) Rudjer Boskovic Institute, 41001 Zagreb, Yugoslavia

a) on leave from Central Research Institute for Physics, H-1525 Budapest, Hungary

1. Introduction

NA35 is the only experiment of the CERN heavy-ion program which potentially provides nearly 4π coverage and momentum measurement for charged particles. However, as outlined in a previous memorandum to the SPSC [1], the high particle density in the forward hemisphere makes it difficult in sulphur-nucleus reactions to analyse particles forward of mid-rapidity in the streamer chamber. It is therefore proposed to build a Time Projection Chamber (TPC) and install it downstream of the vertex magnet (see Fig. 1), where it will complement the acceptance of the streamer chamber.

A sketch of the proposed TPC is shown in Fig. 2. The overall dimensions of the sensitive volume will be 2500 x 1000 x 1400 mm^3. Initially we intend to equip one third of the detector for complete tracking and dE/dx readout, the remainder of the detector will be instrumented for tracking only (see Fig. 3).

The TPC will enable us to analyse large numbers of events easily and quickly since it is positioned outside the magnetic field and the tracks are therefore straight lines. Using the measured characteristics of the events, the TPC can serve as a highly selective offline trigger to define interesting event samples for complete but much slower measurement in the streamer chamber.

The proposed TPC will also serve as a developmental prototype for a large solid angle detector envisaged for the future Pb-beam program. In particular it will be possible to study the performance with respect to tracking accuracy, two-track resolution and dE/dx measurement in a high multiplicity - no magnetic field environment using pad readout only.

In order to be able to construct the TPC for 1990 the design is based on proven technology which was developed for the ALEPH experiment and which is available in the MPI-Munich workshops.

2. Physics Motivation for the TPC in NA35

So far we have studied O + Au and S + S reactions in the laboratory rapidity region $y_{Lab} < 4$ and 3, respectively. We have already obtained three important results from the individual track measurements in the streamer chamber [2]:

(i) The inclusive transverse momentum distributions show a non-thermal behavior [3].

(ii) The radius of the pion emission region, obtained from Bose-Einstein correlations, seems to be twice as large as the oxygen projectile radius [4].

(iii) The ratio of strange particle production to pion production is not increased in central O-nucleus compared to p-nucleus collisions [5].

The slow measurement rate for streamer chamber pictures has, up to now, limited the statistical accuracy of the experiment and has so far precluded more detailed investigations. From the existing results, it appears that if the Quark-Gluon-Plasma (QGP) is produced with O,S ions this either happens rarely or leads to subtle signals. Even with the planned increase of the streamer chamber picture measuring speed by a factor of 10 - 20 (see [1]) an improved sensitivity of the experiment is desirable. Moreover the analysable rapidity region should be extended beyond $y_L = 3$, specifically for S + heavy-nucleus reactions which may be the most likely ones to create QGP. To meet these demands, we propose to add a downstream TPC to the present detector. This TPC will have the following properties:

(i) Tracking and momentum measurement for charged particles in the forward hemisphere

(ii) dE/dx measurement in the relativistic rise region with 6% accuracy in one third of the detector

(iii) Data recording rate of 20 events/sec, which is a factor 20 increase with respect to the streamer chamber.

2.1. The TPC used in Conjunction with the Streamer Chamber

For the event sample for which both the streamer chamber and the TPC data are recorded, the TPC information completes the phase acceptance of the experiment. The TPC can be used to select a sub-set of events for measurement of the streamer chamber pictures. We intend to look specifically for rare events which could be candidates for QGP production. Using the cluster analysis algorithm developed by the JADE group [6] one might search for a small scale jet structure. For rare events the rapidity distribution for $y_L > 3$ might not be smooth, as usual in high multiplicity events, but might show one or more very sharp peaks. Such fluctuations could be the so called hadron bubbles or hot spots from the hadronisation of supercooled regions of QGP [7, 8]. Using the dE/dx information provided by the TPC, one might select events statistically enriched with protons, antiprotons or kaons.After analysis of the corresponding streamer chamber picture the event can then be examined in full phase space for other QGP signatures.

2.2. The TPC Used for Studies with High Statistical Accuracy

The data from the TPC, which covers the forward hemisphere of the reaction, will be used to address several physics questions with high statistical accuracy. The forward hemisphere is not influenced by target spectator nucleons or products of cascading in the spectator nuclear matter. This region is therefore important for an understanding of the differences between p-nucleus and S-nucleus collisions. So far new effects have been observed in comparing pp and p-nucleus reactions. However, it is not clear whether there is new physics when going from p-nucleus to nucleus-nucleus collisions, since only the $y_L < 3$ region has been studied extensively.

Tracking in the TPC will provide momentum measurements for particles with rapidities $y_L > 3$. Negatively charged particles are mostly produced pions. Positively charged particles contain the incident projectile charge. The difference of the rapidity distributions of positively and negatively charged particles (charge flow) represents an approximate measurement of the rapidity distribution of the projectile fragmentation protons. The knowledge of this distribution is important for understanding the degree of stopping of the projectile energy.

The measurement of two-pion Bose-Einstein correlations in 108 central O+Au collisions has already produced the unexpected result that the emission volume for pions is twice larger for mid-rapidity pions than for backward and forward produced pions. A detailed, high statistics study of these correlations holds the potential for elucidating the space-time structure of the hadronization process [9] or even providing indications of QGP production [10]. The proposed TPC offers the required measuring accuracy, two-track resolution and event rate to perform such an investigation in the rapidity range $y_L > 3$.

Correlations have also been proposed to show specific signals, if the QGP were produced. Jet structures and large fluctuations in the particle density in small rapidity intervals were discussed above (section 2.1). The study of intermittency [11], i.e. the growth of multiplicity fluctuations in decreasing phase space regions, can be studied for $y_L > 3$ with high statistical accuracy. As pointed out in [12] the measurement of these fluctuations, in particular when performed in small intervals of rapidity and azimuthal angle ϕ can provide valuable tests of hadronisation models or even show an indication of QGP [13].

2.3. Usefulness of the dE/dx Measurement

One third of the TPC will be fully equipped electronically to allow the measurement of the energy loss dE/dx of particles in this region with an accuracy of 6%. While a resolution of 3% would be necessary for complete track by track identification in the relativistic rise region, the 6% accuracy obtainable with 1.2 m track length is still very useful for many purposes.

Identified particle spectra can be extracted on a statistical basis. Proton spectra are important for an understanding of the stopping of the incident energy. Antiproton production has been advocated as a reference with which to compare antilambda production (measured in the streamer chamber) [14]. QGP production is expected to show up as an increase in the $\overline{\Lambda}/\overline{p}$ ratio. Specific differences in the K^+ and K^- transverse momentum spectra have also been proposed as an indication of QGP formation [15].

3. Basic Design Concept

3.1. Detector Location

Two principal locations for the TPC are anticipated: a) in the forward direction, centered on the beam, with the beam passing through the TPC, and b) on one side of the beam direction, just clearing the beam. Location a) gives acceptance for charged particles complementary to that of the streamer chamber and will permit a much more complete characterization of individual events than previously was possible. Location b) will accommodate higher beam intensities and a more selective trigger. While the TPC acceptance in this location will be predominantly for one sign of particle charge, it will extend farther downwards in rapidity than that for location a). This location will especially be suited to studies of Bose-Einstein correlations, either in conjunction with the streamer chamber or in stand-alone operation.

Measurements will also be made with the vertex magnet field reduced from its normal 1.5 T to a value of 0.5 T. This will extend the acceptance for pions downwards beyond mid-rapidity even in location a). It will also be useful for measurements at 60 GeV/A.

3.2. Limit on Beam Intensity/Interaction Rate

The usable beam intensity will be determined by the time needed to clear the TPC after an event. The electron drift velocity in neon is $3cm/\mu s$, so that a beam track at the center of the chamber requires $20\mu s$ to clear. An event filling the entire TPC requires $40\mu s$ to clear. Thus in location a) where the beam passes through the TPC, the beam intensity should be limited to 10^4 per second for 20% pile-up (it should be noted that pile-up will easily be recognizable on vertex reconstruction). With a 1% interaction thickness target there will be 100 minimum bias events per second, of which (for simplicity of argument) a loose trigger might select 20 central triggers per second for readout. In location b) the interaction rate should be limited (for a maximum of 20% pileup) to 5000 minimum bias events per second. Here a much harder central trigger could be used, and a beam intensity of $5 \cdot 10^5$ could be used with the same 1% interaction length target. These operating rates are both compatible with simultaneous streamer chamber operation (with a lower trigger rate for the streamer chamber).

3.3. Space Charge

It will be shown in Appendix 1 that these beam intensities and event rates do not lead to important space charge distortions of the drift field due to accumulation of positive ions in the drift volume. We have carried out calculations both for 10^4 sulphur beam tracks per second inside the TPC and for a realistic (FRITIOF) distribution of secondary particle tracks in the TPC from 10^4 central events per second with the beam passing outside the TPC. We find that both operating conditions are acceptable. Our calculations are quantitatively consistent with recent measurements made under comparable conditions in the E810 TPC at BNL.

3.4. Data Flow and Storage

We assume 20 central triggers per second during the spill. With about 200 tracks in the TPC each central event contains, after zero suppression, about 150 kbytes of information. For a 4 second spill this amounts to 12 Mbytes which must be buffered and read out during the 14 second cycle time of the accelerator. The input rate of 3 Mbytes/s is easily handled by fastbus. While the 750 kbyte/s write speed of standard high performance 6250 bpi tape drives would match the output rate if two tape drives were used, the 200 Mbyte capacity of the tapes is unacceptable, since a tape change would be needed every 200 seconds. We therefore plan to use four helical-scan 8mm tape drives each with a write speed of 250 kbytes/s and a capacity of 2 Gbytes. One tape would be filled every 2000 seconds. The cost of the four tape

drives is about $\$20K$, and the cost of tape will be \$400 per day. This method has been tested and utilized in the NA35 experiment for the CCD cameras. At this data rate approximately 20,000 events per hour can be recorded, or 500,000 per day.

3.5. dE/dx Measurement

The six identical TPC modules will each have 30 rows of 4cm-long pads. Two modules will initially be instrumented for complete readout. In addition to simplifying track reconstruction and providing enhanced momentum resolution, this will allow dE/dx particle identification in the relativistic rise region. Measurements by Lehraus et al. show that dE/dx resolution of 6% should be achievable, sufficient to identify individual pions over a large region of phase space. It will also allow identification of kaons and protons on a statistical basis (i.e., not track-by-track but sufficient to extract inclusive spectra or to make statistical corrections to other quantities such as Bose-Einstein correlations that depend on particle identification. In the other four modules of the TPC, electronics will be provided at this stage only for 6 rows of pads for tracking. Even in these modules dE/dx information will be sufficient to reject the unresolved e+e- track pairs resulting from photon conversions in the TPC gas or in the entrance window. The extraction of both tracking and dE/dx information from the pads rather than using the pads for tracking and the wires for dE/dx is dictated by the multiple hit situation on the wires. Measurements on the PEP-4 TPC have shown that the pads give dE/dx resolution comparable to that achieved with the wires. Another TPC using pad readout only, with 24000 pads, is under construction for use in 1991 at LBL's Bevalac. Appendix 2 provides a summary of relevant measurements and references on dE/dx resolution.

3.6. Operation Without Magnetic Field

Since the most familiar time projection chambers have been designed for use in magnetic fields, we give a brief discussion of the advantages and disadvantages of not having a magnetic field in our application. The presence of a magnetic field is not an intrinsic requirement for successful operation of a TPC, but some advantages accrue when a "fast" gas such as argon/methane is employed. Then diffusion of the secondary electrons in the plane perpendicular to the field is reduced, and the effect of radial electric field components in the drift volume such as those due to space charge is also reduced. In the drift direction the magnetic field does not help, diffusion in fact being made worse by the use of a fast gas. Negative aspects of the magnetic field include large E x B effects near the the gating grid and sense wires. In our magnetic-field-free application we choose a slower gas, neon/methane. Then

diffusion is reduced to a satisfactory level, both transversely and longitudinally. The development of effective gating grids has reduced the effects of space charge to manageable proportions, as discussed below. The price to pay for the use of a slower gas is that the electric field gradient in the drift volume has to be increased. This, and count rate considerations, prevent the use of a very slow gas such as those used in high- resolution vertex detectors. Neon provides a good compromise for the present detector. Appendix 3 gives a comparison of the performance of Ne/CH_4 with that of other frequently-used gases.

3.7. Choice of Gas

In addition to optimization of the performance of the TPC, especially the reduction of diffusion, discussed above and in Appendix 3, there are additional reasons for the choice of neon rather than argon. The reduction in Z markedly reduces the number of photon conversions and delta rays produced in the gas as well as the amount of multiple scattering. The lower dE/dx leads to lower space charge accumulation. There is a small but acceptable loss in tracking resolution, but (remarkably) an improvement in dE/dx particle discrimination in the range of particles and energies relevant to the present experiment [16]. Furthermore, for gas pressures near atmospheric, the particle discrimination achieved in a given length of detector is roughly independent of the pressure [16], so that atmospheric pressure is a natural choice. This is a result of the fact that while the percentage dE/dx resolution achieved improves as the pressure is increased it is counteracted by a diminution of the relativistic rise.

3.8. Track Measuring Accuracy

The track measuring accuracy will be about 300 microns horizontally and 200 microns vertically for tracks near the beam direction, where tracking accuracy is most critical (see Appendix 4 for the formulas used in the calculation). At other angles it depends slightly on diffusion but more significantly on the "tanα" effect in the horizontal plane and the analogous "tanλ" effect in the vertical (non-bend) plane. In the vertical direction, the dip angle λ is always less than 0.1, and the accuracy will be better than 400 microns everywhere. In the bend direction, values of tanα will typically be up to 0.1 in the forward detector location, and up to about 0.2 in the side detector location. The horizontal tracking accuracy will deteriorate to about 800 microns and 1.6mm respectively at the sides of the detector. This has no significant effect on the ability of the detector to measure the physics quantities

of interest. The momentum resolution achieved is approximately dp/p= 0.001·p (GeV).

3.9. Two Track Resolution

The ability to resolve close tracks is important in order to avoid random pile up of tracks in regions of the detector where the track density is high and to permit the study of Bose-Einstein correlations. The latter involves measurement of pairs of like-sign particles differing very little in momentum and whose tracks therefore are close together in the detector. We define the two track resolution by the (nearly gaussian) distribution of signals along a pad row or along a series of time samples in the drift direction. If two tracks are separated by less than about three standard deviations of this distribution, they will be difficult to resolve. Near the beam direction, the standard deviation of the distribution is about 4.0 mm horizontally and 2.2 mm vertically resulting in a two-track separation capability of about 1 cm. At other locations in the TPC these values vary slightly, but even at the extremes of the detector deteriorate by a factor less than about 1.5.

A brief comparison of the performance expected of the TPC with that achieved by the NA36 TPC is given in Appendix 5.

4. Performance of the Detector

4.1. Acceptance

The acceptance calculations were carried out in two steps

(1) Particles were generated uniformly in rapidity y and transverse momentum p_T. This calculation was used to derive y/p_T maps of the acceptance.

(2) Particles were generated with the FRITIOF event generator simulating central S + Au collisions at 200 GeV/nucleon incident energy. These data illustrate the number of particles to be expected in the TPC. They also show that the fraction of particles which cannot be resolved is small.

The target position was 10 cm upstream of the streamer chamber (see Fig. 1). Particles were traced through the magnetic field of the vertex magnet and then extrapolated to the location of the TPC. It was assumed that all those particles which emerged from the high track density "beam pencil" region could be measured in the streamer chamber. From our measuring experience we expect the difficult region of the "beam pencil" to have a width of ±30 cm (in the bend plane of the magnet) and a height of ±10 cm (vertical) at the exit of the streamer chamber.

Particles were defined as accepted by the TPC if their trajectory passed through the full length of the sensitive volume (2.4 x 1.0 x 1.2 m^3 extension in the horizontal x vertical x longitudinal direction). The TPC was positioned with its front face 5.1 m downstream from the target, 4 m from the magnet center.

First we show results of calculations with the TPC centered on the beam line. Fig. 4 shows contour plots of the acceptance in the streamer chamber (b,d,f) and in the TPC (a,c,e). The combined acceptances cover the full p_T/y phase space region. Histograms of the particle density dN/dy of different particle species predicted by the FRITIOF model are presented in Fig. 5. The full histograms show all generated particles, the dashed histograms those particles which are accepted by the TPC and the dashed-dotted histograms the particles which have nearby neighbors closer than 1 cm and provide an estimate of the fraction which cannot be resolved. Clearly this latter fraction is small and can be corrected for in the measured particle spectra.

In stand alone operation of the TPC for high statistics studies of Bose-Einstein and other correlations it is desirable to cover a larger rapidity range with the TPC. This can be done for the particles of one sign of charge by displacing the TPC sideways in the bend direction of the magnet. Fig. 6 shows that with a shift of 120 cm good acceptance is now obtained for π, K, $\overline{p}$ with rapidities above 3.0, 2.2, 2.0 respectively.

The acceptance can be extended further down to mid-rapidity pions by reducing the field strength of the vertex magnet to 0.5 T. Fig. 7 illustrates that in this configuration the acceptance is large for pions with rapidities above 2.5. The momentum measuring accuracy will still be acceptable for the mid-rapidity pions since their momenta are not too high.

4.2. Discrimination against Background

Since the TPC requires a knowledge of the vertex location in the bend plane in order to determine the momentum of a particle it is important to study what happens on reconstruction of tracks in the TPC that do not originate from the primary vertex. Sources of such tracks include neutral strange particle decay, decay in flight of pions and kaons, and photon conversion in the streamer chamber and other materials in front of the TPC.

In order to test this we proceeded in two steps. We first studied the reconstruction capability of the detector for charged tracks originating in the target, generated by FRITIOF. These particles were swum through the magnet into the TPC taking into account multiple scattering, and measurement errors were assigned according to

the known resolution of the detector. We then reconstructed the particle momenta assuming the known vertex location in the bend plane (horizontal) and studied the accuracy with which the vertex was reconstructed in the non-bend direction (vertical). We found a typical accuracy of a few mm.

We next studied background by running FRITIOF-generated events through GEANT, selecting particle decay and photon conversion as the secondary processes most likely to cause difficulty. We determined the paths of the resulting tracks through the TPC and extrapolated them back into the magnet as if they had originated, in the bend plane, from the primary vertex. This does not give the correct momentum for the observed particle, but it does allow a calculation of the apparent vertex location in the non-bend direction which can be used as a criterion for the rejection of tracks. We found that by this means we could eliminate two thirds of the secondary tracks which reach the TPC. The remainder constitute about 5% of the total measured tracks. Corrections for these will have to be made by Monte Carlo methods.

4.3. Bose-Einstein Correlation

The study of Bose-Einstein correlations requires the measurement of the correlations of like-sign particle pairs with small momentum differences. These differences are usually analysed in the rest system of the particle pairs, where therefore high momentum measuring accuracy and two particle separation power are required. The width of the correlation peak decreases with increasing size of the particle source and a resolution of better than $\Delta p_{cm} \approx 20$ MeV is required, for example, to analyse a source size of 10 fm.

To illustrate the useful acceptance of the TPC for Bose-Einstein correlation studies, we assumed a required resolution power of $\Delta p_{cm} \approx 30$ MeV, corresponding to a radius of about 7 fm. In the calculation we took into account the measuring accuracy in the TPC (6 pad rows, smearing due to diffusion and pad response function) as well as multiple scattering of particles up to and including the TPC entrance window. These effects cause an apparent change of the track parameters in the TPC and thus result in a change of the computed particle momentum vector at the production point in the target. Figs. 8, 9 present the results for the side position of the TPC with the magnetic field set at 1.5 T and 0.5 T respectively. The full line shows the 1 cm two-track resolution limit for like-sign particle pairs with a momentum difference $\Delta p_{cm} = 30$ MeV. The curve of constant measuring accuracy $\delta p_{cm} = 30$ MeV is represented by the dashed line. The dotted lines show where the geometrical acceptance reaches 20 %. The useful regions for Bose-Einstein

correlation studies are the regions bounded by the three curves, i.e. $3.5 \lesssim y \lesssim 4.5$ (Fig. 8) and $2.5 \lesssim y \lesssim 3.5$ (Fig. 9) with 1.5 T and 0.5 TG field respectively.

We also carried out a simulation using an actual correlation function that might be expected in central S + Au collisions assuming a radius of 10 fm for the pion source, which might be expected if the results of [4] are confirmed. For this purpose we generated events with 200 negative pions distributed randomly according to the inclusive p_T/y distributions measured in our experiment. Close particle pairs were weighted by gaussian correlation functions with widths R = 10 fm and λ = 1. The particles were then traced through the detector, the measuring resolution was applied and pairs closer than 1 cm in the TPC were eliminated. Fig. 10 shows the projections of the 2-dimensional correlation functions $C_2(Q_T, Q_L)$ together with the results of a maximum likelihood fit for an event sample of 7400 events. Such a sample corresponds to about one hour of data acquisiton. The generated particle momenta were used in Fig. $10a, b$ and the effects of detector resolution are included in Fig. $10c, d$. Some reduction in the fitted values of the coherence parameter λ and the longitudinal radius R_L are observed which may be corrected for in the data analysis.

4.4. dE/dx Measurements

So far we have not performed a full-scale Monte Carlo simulation of the TPC response to the energy loss of particles. This will be required before we determine which part of the detector it will be most useful to equip with dE/dx capability for the initial operation. However, we have performed a simplified calculation to demonstrate the utility of the method even with our limited resolution.

We used FRITIOF to generate particles for S + Au central collisions at 200 GeV/A. For each particle within the TPC acceptance and with momentum between 10 GeV/c and 50 GeV/c we determined the expected value of the energy loss (truncated mean) using the curves in Fig. 16 of Appendix 2. We then chose a "measured" energy loss by random selection within the expected gaussian distribution. This was used to deduce a "measured" value for the velocity. The particle momentum, after smearing to allow for multiple scattering and measurement accuracy, was then combined with this velocity to provide the "measured" mass. Fig. 11 shows the resulting mass distribution for negative pions, kaons and antiprotons.

The mass distributions of pions,kaons and protons overlap, of course, but after making mass cuts to select certain particles one can determine on a statistical basis the "purity" of the selected sample. For example, within a mass interval $m_1 < m <$

m_2 near the K mass, we define the purity P of the kaon sample as

$$P = N_K/(N_\pi + N_K + N_p)$$

where N_K,N_π,N_p are the numbers of K, π, and p produced by the event generator, that fall within $m_1 < m < m_2$ given the limited dE/dx-resolution. In this example we also define the acceptance ratio R for kaons as

$$R = N_K/N_K^{tot}$$

where N_K is, as before, the number of kaons which fall within $m_1 < m < m_2$, and N_K^{tot} is the total number of kaons.

In Table 1 we give the acceptance ratio R and purity P for particles produced by our event generator, within the acceptance of the TPC and within some specified momentum and mass intervals:

Table 1 - Particle identification capabilities of the TPC

Particle	Mass (GeV)	Momentum (GeV/c)	Acceptance R(%)	Purity P(%)
π^-	.01-.4	10 - 50	95	96
K^-	.4 -.7	10 - 50	54	58
p^-	.65-2.7	10 - 50	84	71
π^+	.01-.4	10 - 50	89	89
K^+	.3 -.6	10 - 50	42	25
p	.8 -2.	10 - 50	54	85

From this table we learn, for example, that by applying a cut on the mass-spectrum given by 0.8 GeV < m < 2.0 GeV, we can select protons with 54% efficiency and can expect that 85% of the particles selected actually are protons. We note that the most difficult particle identification is for K^+, and that it is more effective for the negatively charged species. This is because of the large numbers of protons present in the 10 - 50 GeV/c momentum range.

Given this mass resolution we are quite confident that we can obtain useful inclusive spectra for most of the above particles. It also seems the acceptance ratios and purities might be high enough for special studies such as, for example, two-antiproton interferometry.

4.5. Φ MESONS

It is interesting to investigate whether it would be possible with this TPC to measure Φ mesons via their K^+K^- decay mode, to obtain further information on strange particle production. To test this, we generated a sample of Φ mesons from central S + Au collisions using FRITIOF, and follow the decay particles through the magnet into the TPC taking into account multiple scattering. We then reconstructed the decay particles to the vertex, allowing for measurement errors, and obtained the measured Φ masses. We similarly generated the combinatoric background from all charged particles, assumed for this purpose to be K^+,K^-.

From this preliminary study we can draw three conclusions:

a) the momentum resolution of the detector is sufficient to reconstruct the Φ mass with an uncertainty comparable to its natural width;

b) the K^+ and K^- produced in each central S+Au collision generate sufficient combinatoric background that identification of individual Φ mesons will in general be impossible - the signal to noise ratio being approximately unity;

c) the combinatoric background due to pions (if not identified) is about one hundred times the signal.

Nevertheless, the expected yield of Φ mesons is expected to be quite large (of the order of 1 per event) so that quite good statistics for inclusive studies should be available. In the region of the TPC instrumented for dE/dx we expect to be able to eliminate 90% of the pions, and reduce the combinatoric background due to pions by a factor of 100, down to the irreducible level due to $K^{+/-}$. Our study is not yet complete, and these results may be different in selected regions of phase space, but we conclude that Φ meson inclusive measurements with this detector will be a practical avenue to pursue further.

5. Detector Description

A sketch of the proposed TPC is shown in Fig. 2. The overall dimensions of the drift volume are approximately 2500 x 1000 x 1400 mm^3 with a vertical drift length of 1000 mm. The six independent readout modules are placed at the top of the field cage and cover an area of 2370 x 1260 mm^3. The dead strips between the modules are 30 mm wide in beam direction and 24 mm perpendicular to it. During the time which is needed for the trigger and to open the gating electrodes (approx. 3 μs) 10 cm of the event are lost [17]. To compensate for this the whole detector is displaced by the same amount in the drift direction.

The TPC will be mounted in a large air-conditioned hut such that it can be moved between different positions (centered on the beam or moved to the side) within a short time.

The design of the readout modules is based on the ALEPH-TPC design [18],a rigid Aluminium-G10 sandwich structure. In some respects it becomes simpler, due to the fact that there will be no wire readout and that the shape is rectangular. The pad plane (768 x 600 mm^2) is completely covered with 5.5 x 39.5 mm^2 pads with .5 mm gaps between them. There are 128 pads in a row and 15 rows for a total of 1920 pads per chamber module. A schematic drawing of a readout module is shown in Fig. 12. A more detailed design drawing of the pad and wire arrangement is shown in Fig. 13.

For better 2-track resolution and position accuracy the gap between pad plane and sense wire plane is 3mm while the distance of the sense wire plane to the grid cathode is 4mm. The 20μ sense wires with 4 mm pitch are interspaced with 125μ field wires. With an additional gating electrode we expect a suppression factor $> 10^4$ for ions drifting back into the drift volume. The preamplifiers are mounted directly on the readout modules and their sockets are water cooled. An additional air ventilation into the sandwich structure avoids heating up the pad plane and the gas.

From the experience gained in the production of the ALEPH-TPC we expect a pad-to-pad position precision of ± 30 μm and similar values for the planarity of the pad plane and parallelism between the sense wire plane and the pad plane or grid cathode.

About 200 charged particles are seen by the TPC in a typical S+Au central collision. To minimize the background from conversions, scatterings and interactions the walls of the fieldcage have to be as thin as possible. But to provide the necessary drift field uniformity one also needs excellent mechanical stability. Both requirements can be met by a Rohacell sandwich structure. A 50 mm thick Rohacell plate is covered on both sides with a 75 μ Kapton foil. The inner foil has a 25 μm copper layer which is etched in stripes to form the uniform drift field. The stripes are 10 mm wide and are separated by 2 mm from each other. The outer surface is also conductive and serves as an additional shielding. The estimated wall thickness is $\leq 0.5\%$ of a radiation length or $< 10^{-3}$ of an interaction length. A prototype is under construction and will be tested in the near future.

To read out the pad signals we are going to use the ALEPH electronic chain with some minor modifications to adapt it better to the requirements of our experiment.

A block diagram of the electronics is shown in Fig. 14. The chain consists of a preamplifier card on the readout module with 16 channels, approx. 30 m cable to the control room, the Time-Projection-Digitizer (TPD) including shaper and FADC with 64 channels each and the ALEPH-Event-builder. The TPD's and the Event-builder are Fastbus modules. A newly developed shaper with larger dynamic range and better saturation behaviour will be used. The FWHM of the shaper signal is 180 ns and the clock frequency for sampling is 15 MHz giving an improved 2-track resolution in drift direction.

The main TPC parameters are summarized in Table 2.

Table 2 - TPC Parameters.

Drift Volume	approx. 2500x1000x1400 mm^3
Readout Area	2370x1260 mm^3
Sampled Track Length	1200 mm
Drift Length	1000 mm
Drift Field Ne(Ar)/10%CH_4	200(115) V/cm
Max. Drift Time Ne(Ar)	30(20) μs
No. of Readout Modules	6
Module Dimensions	790x630 mm^2
Pad Size	39.5x5.5 mm^2
No. of Pad Rows/Module (Total)	15(30)
No. of Pads/Row	128
No. of Pads equipped with Electronics	5376
Gap Sense Wire-Pad (Grid cathode)	3(4) mm
Sense Wire Diameter	20 μm
Field Wire Diameter	125 μm
Sense Wire Voltage [19]	approx. 1200 V

6. Schedule and Cost

6.1. SCHEDULE

A small test TPC is already operating at the MPI in Munich. It is being used for gas and field cage tests and will be installed in the CERN PS T10 beam line in May.

The design of the readout modules is well under way. Materials with long delivery times are ordered or requests for offers are made. Workshop capacity at

the MPI is reserved for the next 14 months. The completion of the first modules is planned for the beginning of 1990 and all are expected to be completed by the end of March,1990.

A prototype for the field cage is under construction and can be tested soon. Then the final design can be made and construction can start.

The main parts for the TPC-hut exist.

The orders for the first 3000 preamplifiers are prepared and they can be delivered within 15 weeks. The delivery of the second 3000 channels is foreseen for the second half of this year. The situation for the shaper is similar. The TPD's will be made by the same company which has worked for ALEPH. For the required 90-100 units a typical delivery time is 10 months.

Parts of the Fastbus system exists and can be used for online software development and readout tests.

The offline software is based on the ALEPH software and is expected to be modified and available within the next 12 months.

6.2. Cost Estimate

The following costs have been estimated for new equipment. We need 5500 channels for equipping 6 pad rows for tracking and all pads in 2 modules completely for dE/dx measurements.

Item	Price (ksfr.)
5500 Electronic channels*	920
7 Readout modules (material cost)	120
Computer	125
Gas system	35
Calibration system	45
Field cage	20
Support	10
	1275
+15% contingency	190
	Total 1465

* ALEPH paid 145,- sfr per electronic channel,including crates, power supplies, cables, etc.. To compensate for expected price increases we assumed a price of 165,- sfr.

The total amount of approx. 1.500 ksfr will be provided in 1989 and 1990 by four institutions of the collaboration: Univ. of Frankfurt, GSI, LBL and MPI Munich.

7. Appendices

7.1. Appendix 1: Space Charge Limitations

Space charge build up is potentially a serious problem in time projection chambers, because of the avalanche multiplication at the sense wires, which may inject as many as 10^4 positive ions back into the drift volume for each electron that is detected. Because of the large size of the detector and the slow drift velocity of the positive ions (about 400 cm/s in our instance) a large net accumulation of positive charge could occur, to produce significant distortions of the drift field. The cathode (Frisch) grid reduces the feedback by a factor of about 10 [20]. The development of active gating grids for time projection chambers [21, 22, 23, 24] has completely eliminated the remaining feedback, no feedback being observed even at a gas gain of 10^5 [25]. The present detector will incorporate such a gating grid so that the space charge in the drift volume will be limited to the primary ionization.

The distorting effect can still be serious in a sufficiently high multiplicity environment or when the beam is allowed to pass through the detector. We have therefore estimated the effects in both instances, and establish limits of beam intensity and interaction rate for undistorted operation.

We have solved Poisson's equation in the drift volume, for a variety of distributions of positive charge, following the procedure of reference [26]. Fig. 15 shows the potential perturbation (given in Volts) produced by the primary distribution of positive ions for a steady beam intensity of 10^4 sulphur ions per second. Shown is a cross section of the TPC at its median plane. The beam enters at the center and positive ions drift downwards (away from the end-cap) to form an essentially continuous sheet of charge in the lower half of the chamber. The track distortion can be estimated as follows: At the entrance and exit faces of the chamber the potential perturbation due to space charge is zero, because of the proximity of the field cage, whose potential is held constant. Thus the curves in Fig. 15 determine the sagitta introduced by the space charge. It is easily shown that the sagitta is given by V/E, where V is the potential perturbation and E is the unperturbed field gradient. Since the drift field is 200 V/cm, an incremental potential of 1.0 V produces a sagitta of 1/200 cm, i.e., 50 μ. In the worst instance in Fig. 15 the sagitta is about 500 μ. This calculation is in quantitative agreement with measurements made in the E810

TPC at Brookhaven, under comparable conditions [27]. The accuracy of track momentum determination in our configuration is mostly dependent on determination of the entrance and exit points of the track, which occur in regions of low distortion. The magnitude of the sagitta therefore overestimates the error due to space charge distortion, and a sulphur beam intensity of 10^4 per second through the TPC can be considered to be a comfortable upper limit.

A single sulphur ion is equivalent to 256 singly charged particles of the same velocity. It is therefore no surprise that a single interaction producing about 200 secondary particles has about the same effect as a beam particle passing through the chamber. We have performed space charge calculations using FRITIOF simulations of events. For the detector location in which the beam passes through the chamber, with at most 100 events per second, the secondary particles make a negligible extra contribution. When the detector location is on one side of the beam direction, with the beam passing outside it, 10^4 interactions per second produce a maximum sagitta of less than 100 μ, which is negligible. The reason that this situation is less severe than that illustrated in Fig. 15 is that the charge is much more uniformly spread through the chamber.

7.2. Appendix 2: dE/dx Measurement

Particle identification by dE/dx measurement in the relativistic rise regime has been used widely and is thoroughly documented [16, 28, 29, 30, 31]. Because the distribution of energy loss has a long tail which does not help to discriminate between particles it is necessary to use a multiple sampling technique in which the detector is subdivided into a large number of samples and to reject samples with unusually large energy loss by taking a truncated mean, typically rejecting from 30% to 60% of the individual signals. The truncated mean has a gaussian distribution. For a given detector it is found empirically that the percentage resolution is constant throughout the relativistic rise. Subdivision of the detector into as many samples as possible improves the resolution only up to a certain point and it is less effective than increasing the overall detector length. No improvement is obtained by making the samples shorter than about 4 cm·atm [28–30, 32], the value we have adopted for the present detector.

The particle separation to be obtained depends on the gas chosen, and on the particles to be distinguished. When separation of electrons is important (such as at LEP), argon is usually preferred. For low-energy applications such as in the Argus detector at DESY, where discrimination of particles below the ionization minimum is more important than in the relativistic rise, gases such as propane are preferred.

For the range of particles and energies in the present experiment, neon provides the best discrimination for a given length of detector [16]. For gas pressures near atmospheric, the particle discrimination achieved in a given length of detector is roughly independent of the pressure [16]. This results from the fact that while the percentage resolution improves with gas pressure there is a diminution of the relativistic rise. This makes atmospheric pressure a natural choice for the present detector.

Fig. 16 shows the relativistic rise for electrons, pions, kaons and protons in $Ne/10\%C_2H_6$ at atmospheric pressure [33]. The measured quantity is the 40% truncated mean of 128 2cm samples. The rise observed is not expected to be sensitive to changes in the conditions of measurement, and provides a good measure of what to expect in our experiment. The curves represent a parameterization of the response, which should depend only on the velocity of the particle.

To find what resolution is to be expected in our detector, we extrapolate from measurements of 64 4cm samples made in reference [33], where it is stated: "In Ne the n-dependence is ... close to $n^{-0.50}$ and seems to be the same for 1, 2, and 4 atm." For 30 samples of 4 cm, we obtain a resolution of 6.0%. This will give a π/p separation of 4.6 s.d. at 15 GeV/c. Such resolution will allow good identification of individual pions, and identification of kaons and protons on a statistical basis.

7.3. Appendix 3: Comparison of Typical Gases

To illustrate the reasons for our choice of Ne/CH_4 we discuss the consequence of choosing a "fast" gas (Ar/CH_4) in which the drifting electrons are not thermalized, a somewhat slower gas (Ne/CH_4), the mixture $80\%Ar/20\%CO_2$ (much used in former times), or a "cool" gas ($80\%CO_2/20\%$isobutane). The salient properties are shown in Table 3 for typical choices of operating electric field.

The most favored gas for time projection chambers is Ar/CH_4. It requires only a low electric field, the drift velocity is fast (allowing a high count rate), and the probability of electron capture is low. The large diffusion is a disadvantage, partly overcome in a magnetic field as a result of the high value of $\omega \cdot \tau$ which reduces the effects of diffusion perpendicular to the drift direction by the factor $\sqrt{1.0 + (\omega \cdot \tau)^2}$, which is 7.1 for Ar/CH_4 and 2.6 for Ne/CH_4.

Table 3 - Properties of some typical gases: The values for Ar are taken from [32]. The other values for gradient, drift velocity, and diffusion are approximate and taken from the figures in [33]. The value of $\omega \cdot \tau$ is for a magnetic field of 1.5 Tesla and its values for gases other than argon are scaled from argon using the drift velocity in the table and formula (1) of [33].

Gas	Gradient V/cm	Electron Drift Velocity cm/μs	Diffusion mm/cm$^{1/2}$	$\omega \cdot \tau$
91%Ar/9%CH_4	115	5.05	0.67	7
90%Ne/10%CH_4	200	3	0.3	2.4
80%Ar/20%CO_2	500	2	0.2	0.6
80%CO_2/20%isobutane	1000	0.8	0.08	0.1

At the other extreme, a cool gas such as 80%CO_2/20%isobutane requires a high voltage gradient, has a slow drift velocity, high electron capture, and no benefit in a magnetic field from a large $\omega \cdot \tau$. Because of the high voltage gradient required it is mainly suitable when the drift occurs only over short distances, and where very low diffusion is of the essence, as in high-resolution vertex detectors.

Taking into account the other considerations pointing to use of Ne/CH_4 for the present application, this gas appears as a practical and near optimum choice.

7.4. Appendix 4: Predicted Track Accuracy and Two-Track Resolution Capability

We present here, for reference, the formulas which we have used to calculate position measurement accuracy and two-track resolution capability. The quantities introduced have the meanings usually used in the literature, except where noted otherwise. The drift velocity is assumed to be 3 cm/μs, and contributions from electronics noise are assumed to be negligible compared with the fundamental physics limitations.

7.4.1. Tracking Accuracy

The standard deviation of the measurement of a single point is given by σ_1^{horiz} in the horizontal (pad) plane and σ_1^{vert} in the drift direction:

$$(\sigma_1^{horiz})^2 = (a^2 + \frac{b^2}{12} + d^2)/(\ell \cdot n_0) + (\ell \cdot tan\alpha)^2/12n_c$$
$$(\sigma_1^{vert})^2 = (\frac{c^2}{12} + d^2)/(\ell \cdot n_0) + (\ell \cdot tan\lambda)^2/12n_c$$

where

a = distance from sense wire to pad plane (= 3 mm)

b = pad width/spacing (= 5.5 mm/ 6 mm)

c = drift distance corresponding to the separation between time samples (= 2 mm)

d = standard deviation of the diffusion (= $300\mu\cdot$ (drift distance in cm)$^{1/2}$)

ℓ = length of pad

n_0 = total number of electrons produced per unit length of track (= 39/cm)

n_c = effective number of clusters for calculating the tan α effect (taken as 8.1 for neon, 4 cm pads, extrapolated from recent ALEPH measurements (private communication, W. Blum))

α = angle in the horizontal plane between the track and the normal to the pad row

λ = angle between the track and the horizontal plane.

7.4.2. Two Track Resolution Capability

The width of the distribution of the signals for a track, along the pad row or along a sequence of time samples for a given pad, is approximately a gaussian, characterized by its standard deviation. It is assumed that two tracks separated by more than about 3 s.d. can be resolved. The standard deviations for the horizontal and vertical directions are given by:

$$(\sigma_2^{horiz})^2 = (a^2 + \frac{b^2}{12} + d^2) + (\ell \cdot tan\alpha)^2/12$$
$$(\sigma_2^{vert})^2 = (\frac{c^2}{12} + d^2) + (\ell \cdot tan\lambda)^2/12$$

7.5. Appendix 5: Comparison with the NA36 TPC

The NA36 collaboration has been the pioneering group to use the TPC technique at CERN in the study of high multiplicity events produced by ion beams. The objectives of the NA36 experiment and the present proposal differ substantially. It is of interest, nevertheless, to present the expected performance characteristics of the NA35 TPC together with the already-achieved performance of the NA36 TPC [34].

	NA36 achieved	NA35 expected
Vertex reconstruction	yes	non-bend direction only
dE/dx resolution	none	6%
Momentum resolution*	0.8%	0.1%
Measurement accuracy:		
along pad/wire row	730 μ	300 μ
in drift direction	1320 μ	200 μ
Two-track separation**:		
along pad/wire row	0.4 cm	1.2 cm
in drift direction	1.2 cm	0.6 cm
product	0.5 cm^2	0.7 cm^2
Suppression of positive feedback***	98%	100%

* $\frac{\Delta p}{p^2}$ with p in GeV/c

** calculated on the same basis for the two detectors

*** The NA36 TPC has a gating grid but so far it has been used only in a static configuration.

REFERENCES

[1] Memorandum to the SPSC Committee on NA35 Status, Plan and Requirements for 1988/90, CERN-SPSC-88-19, SPSC-P-235 (1988)

[2] For a summary see J.W.Harris et al., LBL-26258 (1988), to be published in Proceedings of Quark Matter 1988, Nucl.Phys.A

[3] H.Stroebele et al., Z.Phys.C. **38** (1988) 89

[4] A.Bamberger et al., Phys.Lett. **B203** (1988) 320

[5] A.Bamberger et al., Preprint MPI-PAE/Exp.El. 198 (1989), submitted to Z.Phys.C.

[6] W.Bartel et al. Z.Phys.C. **33** (1976) 23

[7] M.Gyulassy et al., Nucl.Phys. **B237** (1984) 477
L.VanHove, Z.Phys. **C21** (1984) 93

[8] W.Kittel, Proceedings of the XXIV International Conference of High Energy Physics, Munich, (1988) 625
There are a few reported events in a high statistics $\pi^+ p$ experiment at 250 GeV which have upward fluctuations of a factor 10 in the particle density dN/dy.

[9] W.A.Zajc, Nevis Preprint 1384 (1987)

[10] G.Bertsch et. al, Phys.Rev. **C37** (1988) 1896 and G.Bertsch, MSU-Preprint (1988)

[11] A.Bialas and R.Peschanski, Nucl.Phys. **B272** (1986) 703

[12] W. Ochs and J.Wosiek, Phys.Lett. **214B**(1988) 617

[13] J.Dias DeDeus, Phys.Lett. **194B**(1987) 297

[14] M.Jacob and J.Rafelski, Phys.Lett. **B190** (1987) 173

[15] Kang S.Lee et al., Phys.Rev. **C37** (1988) 1452 and 1463

[16] I.Lehraus, R.Matthewson and W.Tejessy, N.I.M. **200** (1982) 199

[17] C.Brand et al., N.I.M. **A252** (1986) 413

[18] see ALEPH Handbook

[19] I.Lehraus, private communication

[20] O.Bunemann,T.E.Cranshaw, and J.A.Harvey, Design of Grid Ionization Chambers,Can. J. Res. **A27** (1949)

[21] P.Nemethy, P.J.Oddone et al.,Gated Time Projection Chamber, N.I.M. **212** (1983) 273

[22] D.A.Bryman et al.,Gated Grid System Used with a Time Projection Chamber, N.I.M. **A234** (1985) 42

[23] S.R.Amendolia et al., Ion Trapping Properties of a Synchronously Gated Time Projection Chamber, N.I.M. **A239** (1985) 192

[24] S.R.Amendolia et al., Influence of the Magnetic Field on the Gating of a Time Projection Chamber, N.I.M. **A234** (1985) 47

[25] K.Foley, Brookhaven E810 Collaboration, private communication

[26] G.J.VanDalen, TPC-UCR-81-2 (1981) and TPC-UCR-82-3 (1982)

[27] A.Etkin et al., Modular TPC's for Relativistic Heavy Ion Experiments, BNL preprint submitted to the 5th International Wire Chamber Conference, Vienna (1989)

[28] A.H.Walenta, Physica Scripta **23**, 354 (1981)

[29] I.Lehraus, N.I.M. **217** (1983) 43

[30] W.W.M. Allison and J.H. Cobb, Ann.Rev.Nucl.Sci. **30** (1980) 253; and W.W.M.Allison and P.R.S.Wright, Formulae and Methods in Experimental Data Evaluation, with Emphasis on High Energy Physics, Vol.2, p.E1, European Physical Society , CERN RD/606-2000, January 1984

[31] I.Lehraus, R.Matthewson and W.Tejessy, N.I.M. **196** (1982) 361

[32] I.Lehraus, R.Matthewson and W.Tejessy, IEEE Transactions on Nuclear Science, Vol. NS-30 (1983) 44

[33] I.Lehraus, R.Matthewson and W.Tejessy, IEEE Transactions on Nuclear Science, Vol. NS-30 (1983) 50

[34] C.R.Gruhn, NA36 extension request presentation to the SPS Committee, July 1988

FIGURE CAPTIONS

1. Layout of the NA-35 experiment showing the position of the downstream TPC.

2. Sketch of the proposed TPC.

3. Layout of the 6 readout modules of the TPC showing only those pads which will be instrumented for readout in the 1990 data taking period.

4. Contour plots (lines spaced in 10 % steps) of the acceptance of the TPC (a,b,c) and the streamer chamber (d,e,f) for pions (a,b), kaons (c,d) and (anti)protons (e,f). The TPC is centered on the beam line and positioned 5.1 m downstream of the vertex magnet center (B = 1.5 T). The obscured "beam pencil" region in the streamer chamber was assumed to have a width of ± 30 cm and a height of ± 10 cm at the chamber exit wall.

5. Particle density dN/dy of pions (a), kaons (b), antiprotons (c) and protons (d) predicted by the FRITIOF model for central S + Au collisions at 200 GeV/A. Full histograms show all produced particles, dashed histograms those accepted by the TPC and dash-dotted histograms the fraction of unresolved particles (nearest neighbor closer than 1 cm). The TPC was centered on the beam line.

6. Particle density dN/dy of negative pions (a), kaons(b) and antiprotons (c) predicted by the FRITIOF model for central S + Au collisions at 200 GeV/A. Full histograms show all produced particles, dashed histograms those accepted by the TPC and dash-dotted histograms the fraction of unresolved particles (nearest neighbor closer than 1 cm). The TPC was offset to the side of the magnetic bend by 120 cm.

7. Particle density dN/dy of pions (a), kaons (b), antiprotons (c) and protons (d) predicted by the FRITIOF model for central S + Au collisions at 200 GeV/A. Full histograms show all produced particles, dashed histograms those accepted by the TPC and dash-dotted histograms the fraction of unresolved particles (nearest neighbor closer than 1 cm). The TPC was centered on the beam line, the field in the vertex magnet was reduced to 0.5 T.

8. Resolution and acceptance limits for close negative-charge particle pairs in

the TPC. The TPC is shifted 120 cm to the side of the magnetic bend, the magnetic field is 1.5 T.

9. Resolution and acceptance limits for close negative-charge particle pairs in the TPC. The TPC is shifted 120 cm to the side of the magnetic bend, the magnetic field is 0.5 T.

10. Projections of the 2-dimensional correlation fuction on the Q_T axis for $Q_L < 50$ MeV (a,c) and on the Q_L axis for $Q_T < 50$ MeV (b,d) for an assumed gaussian source extension of $R_T = R_L = 10$ fm. Results are for 7400 simulated central S + Au events with ideal accuracy (a,b) and with detector resolution effects (c,d). Fit results are shown by the curves and the numbers in the plots.

11. Mass distribution of negative pions (full line), kaons (dashed line) and antiprotons (dotted line) as computed from the momentum and velocity (dE/dx) measured in the TPC.

12. Schematic drawing of a readout chamber of the proposed TPC.

13. Design drawing showing the pad and wire arrangement of a readout module of the TPC.

14. Block diagram of the TPC readout electronics.

15. The potential perturbation produced by a steady beam of 10^4 sulphur ions passing through the center of the TPC. The perturbation is given in volts.

16. The relativistic rise for electrons, pions, kaons and protons in 90%Ne/10%C_2H_6 at atmospheric pressure [33]. The curves represent a parameterization of the response as a function of the velocity of the particle.

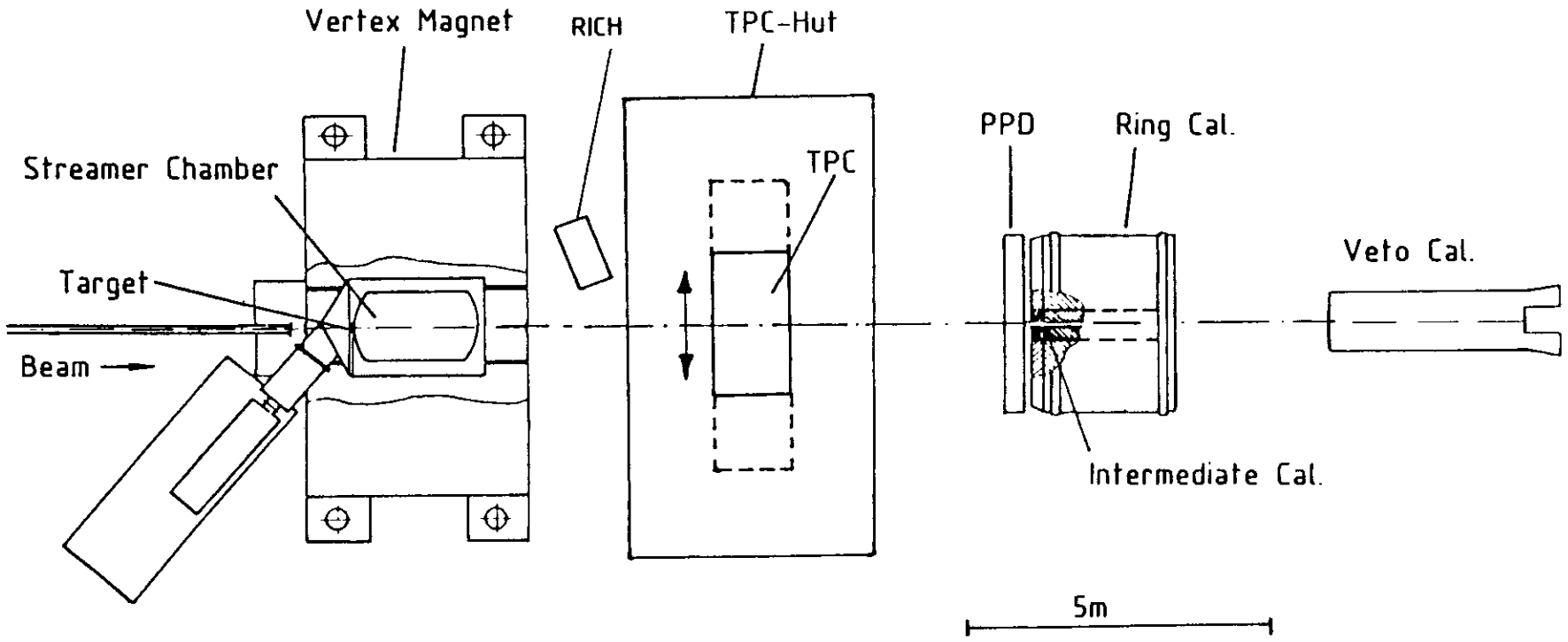
Vertex Magnet
RICH
TPC-Hut
PPD
Ring Cal.
Streamer Chamber
TPC
Target
Veto Cal.
Beam
Intermediate Cal.
5m

Fig. 1

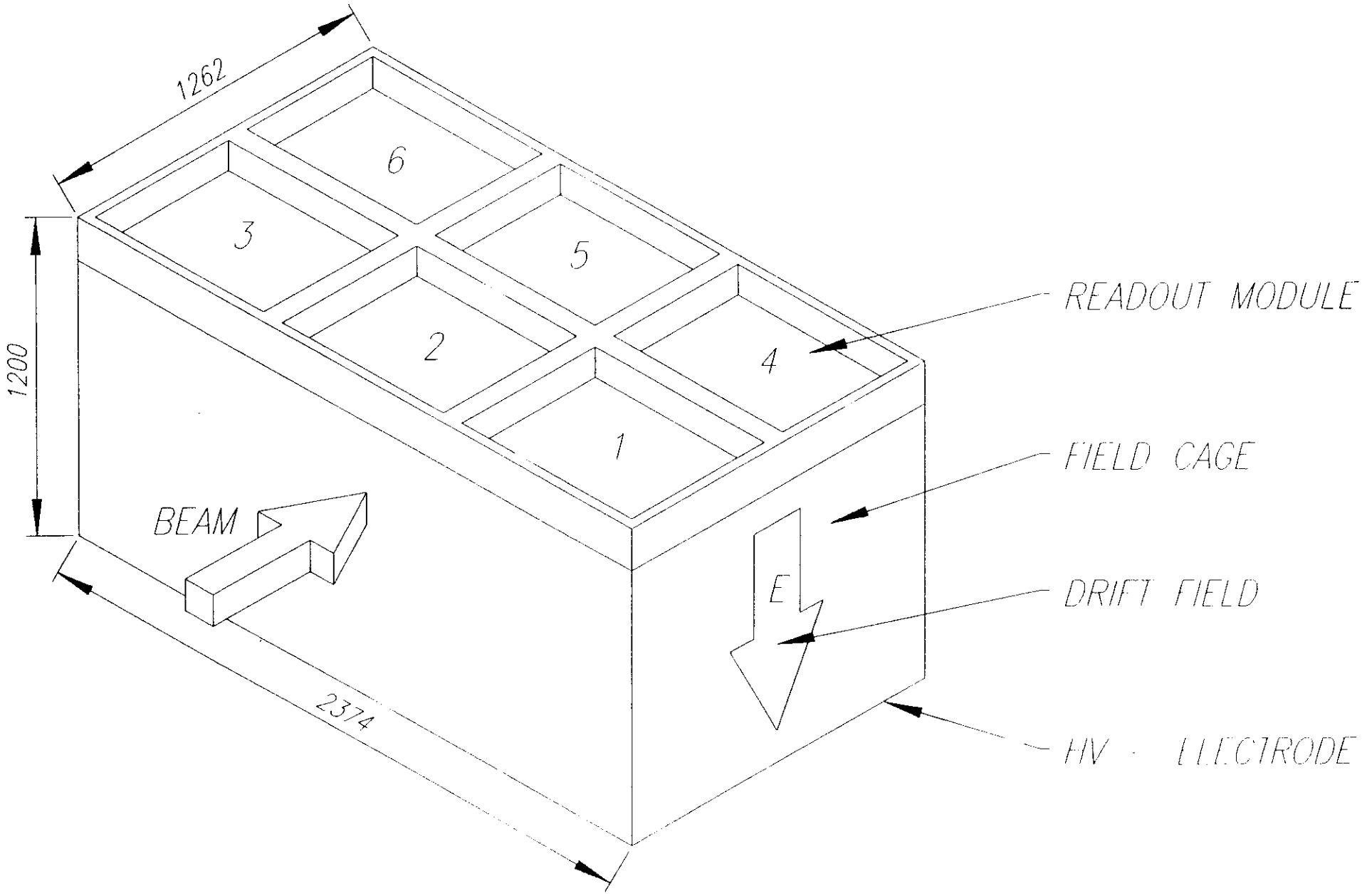
1262
1200
2374
6
3
5
2
4
1
BEAM
E
READOUT MODULE
FIELD CAGE
DRIFT FIELD
HV ELECTRODE

Fig. 2

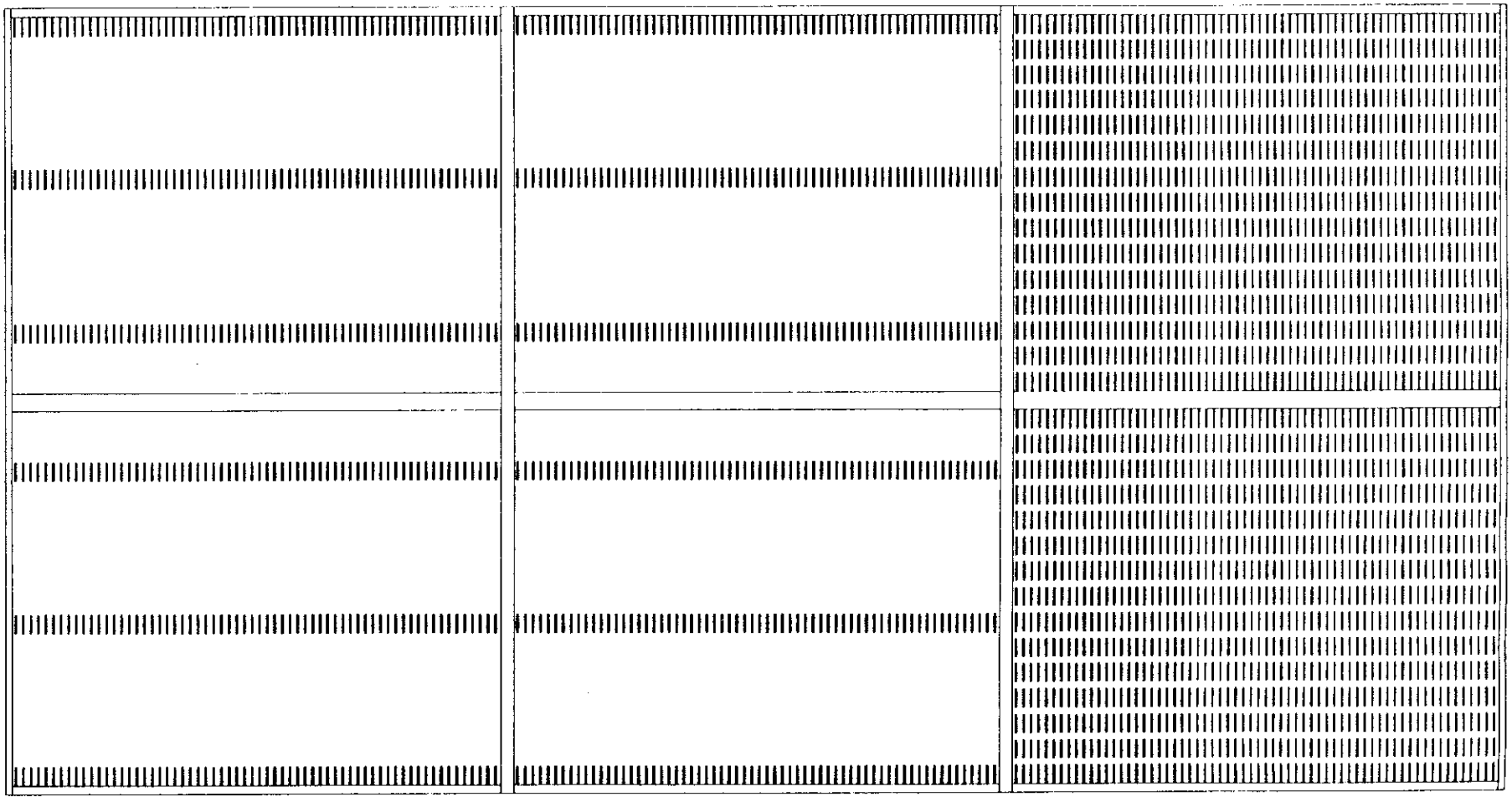

TRACKING ONLY

TRACKING AND dF/dx

Fig. 3

π - ACCEPTANCE

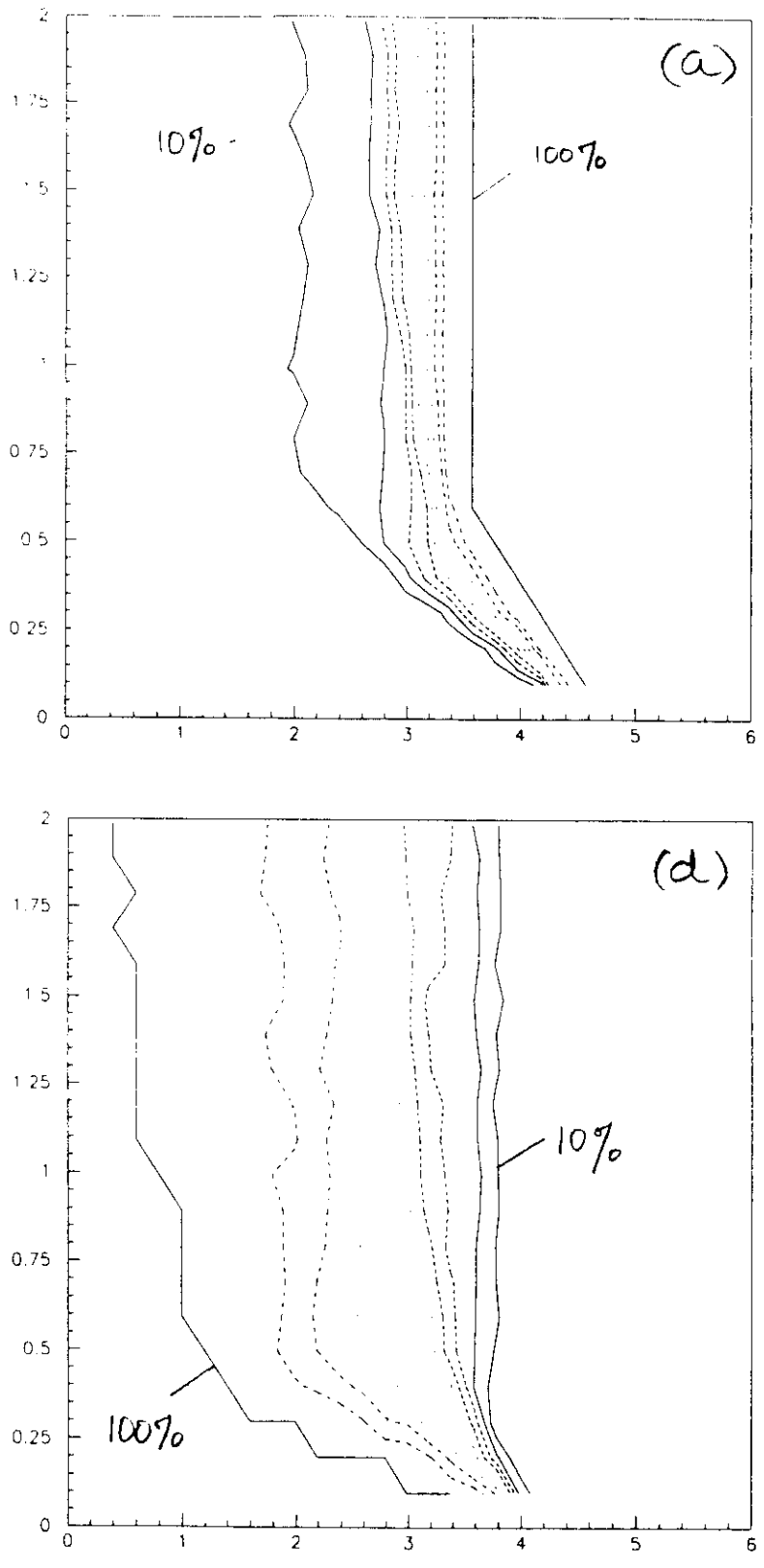

TPC

STREAMER CHAMBER

Fig. 4

K ACCEPTANCE

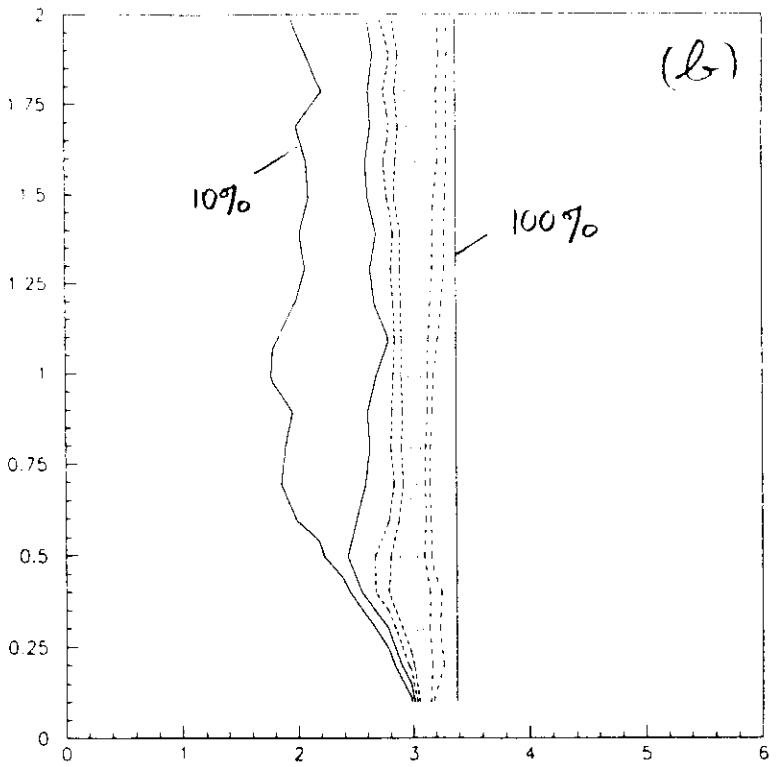

TPC

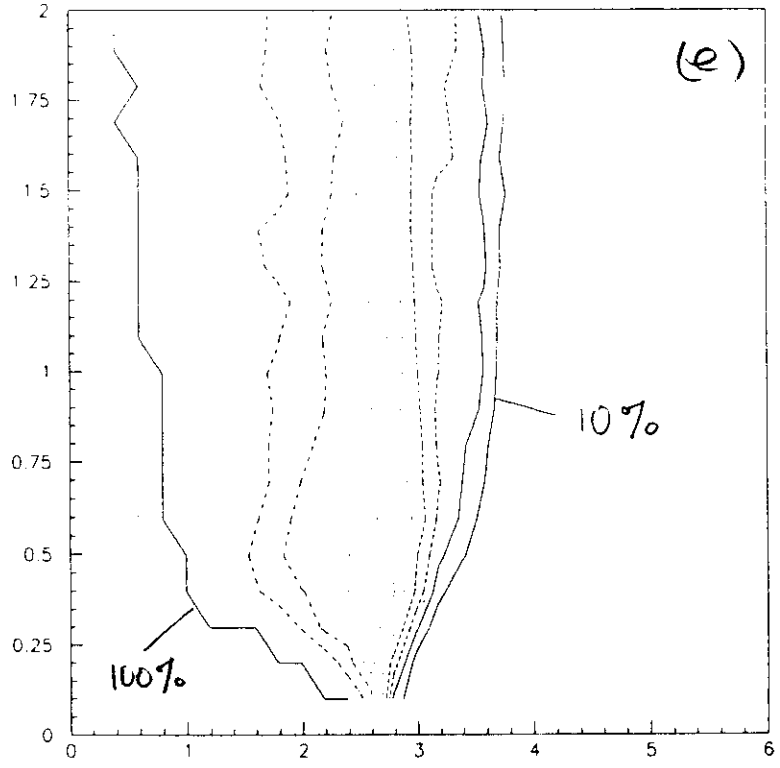

STREAMER CHAMBER

Fig.4

PROTON/ANTIPROTON ACCEPTANCE

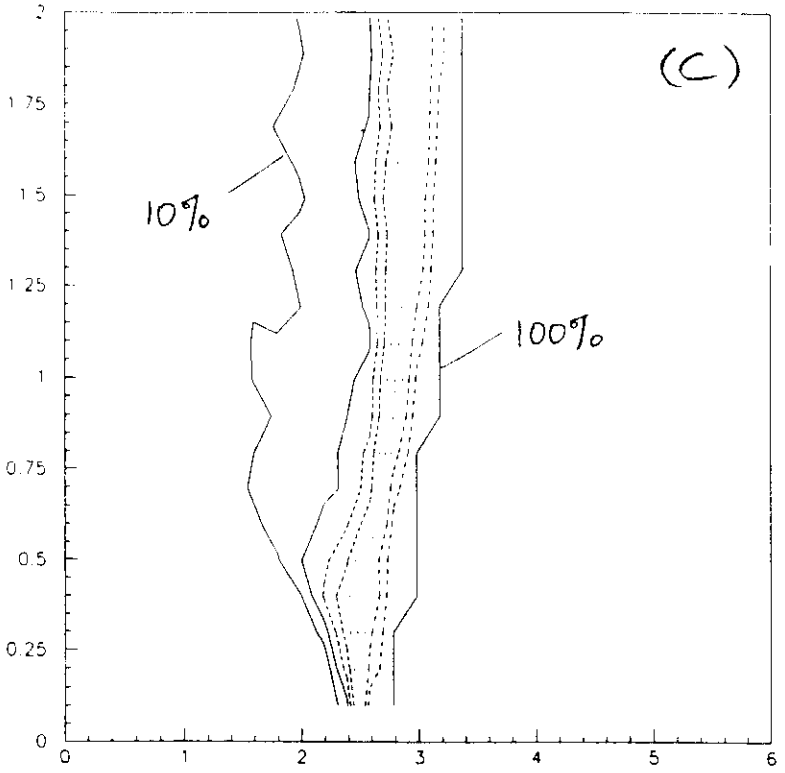

TPC

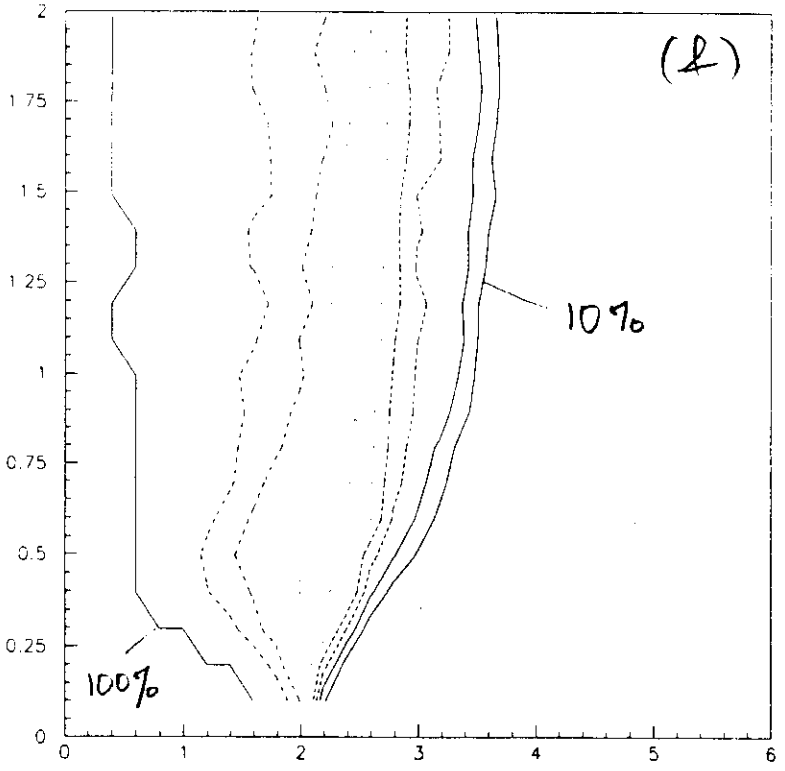

STREAMER CHAMBER

Fig. 4

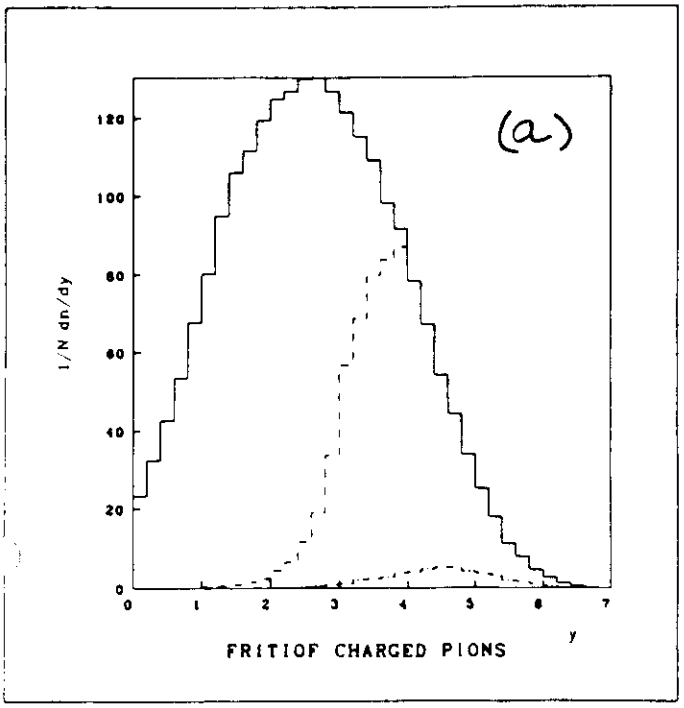
(a)
1/N dn/dy
y
FRITIOF CHARGED PIONS

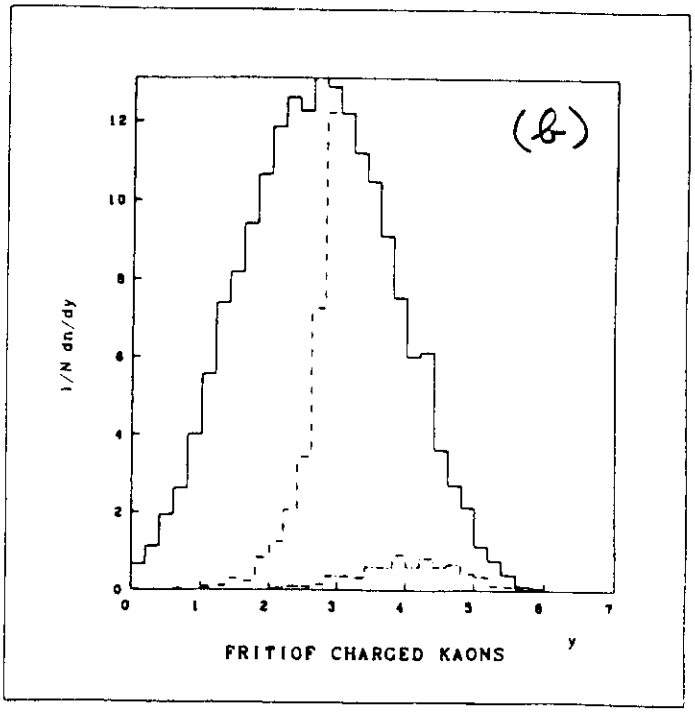
(b)
1/N dn/dy
y
FRITIOF CHARGED KAONS

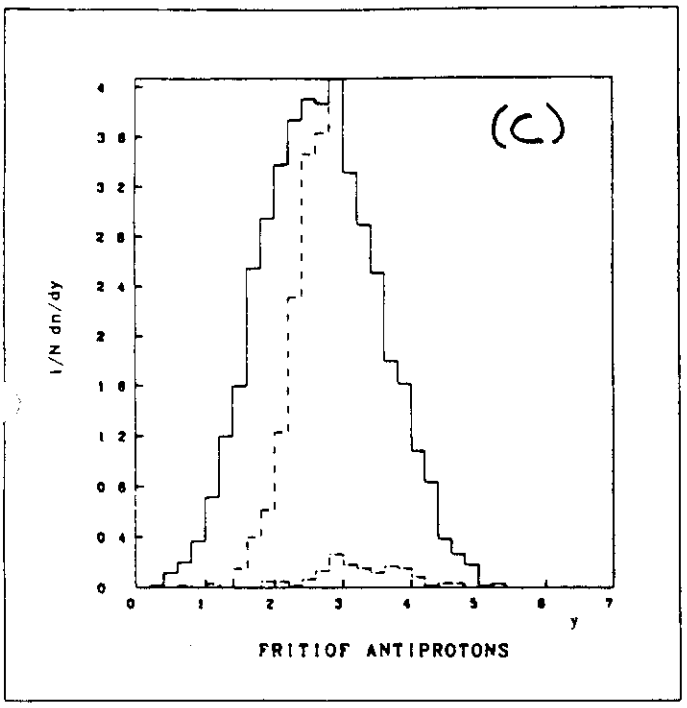
(c)
1/N dn/dy
y
FRITIOF ANTIPROTONS

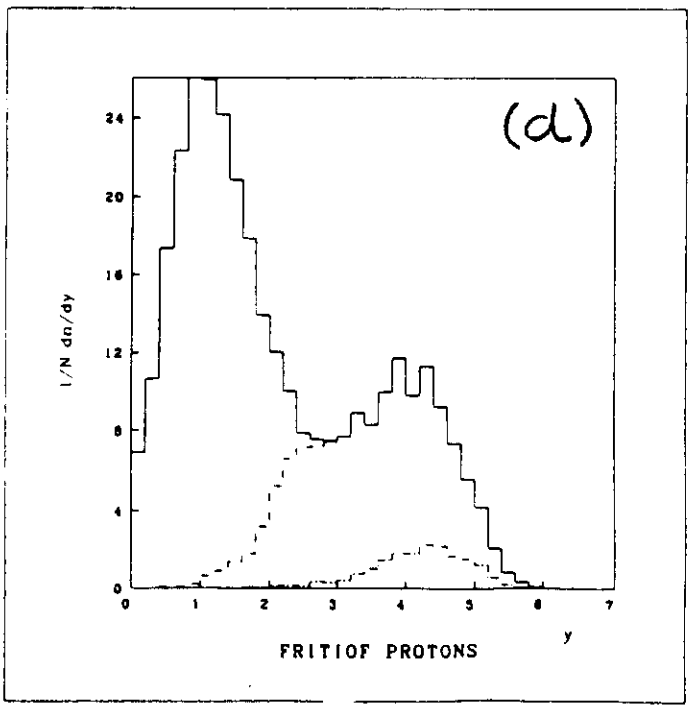
(d)
1/N dn/dy
y
FRITIOF PROTONS

Fig. 5

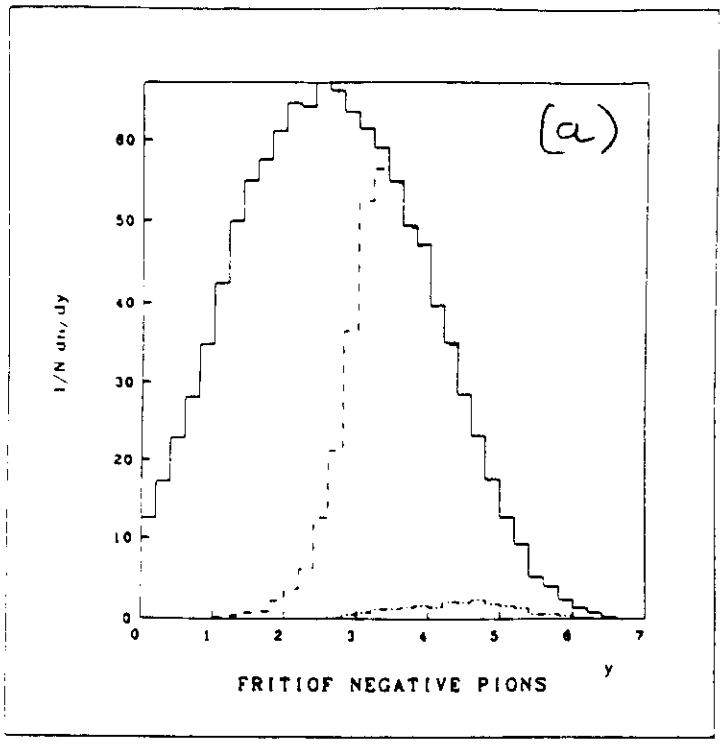
(a)
1/N dn/dy
y
FRITIOF NEGATIVE PIONS

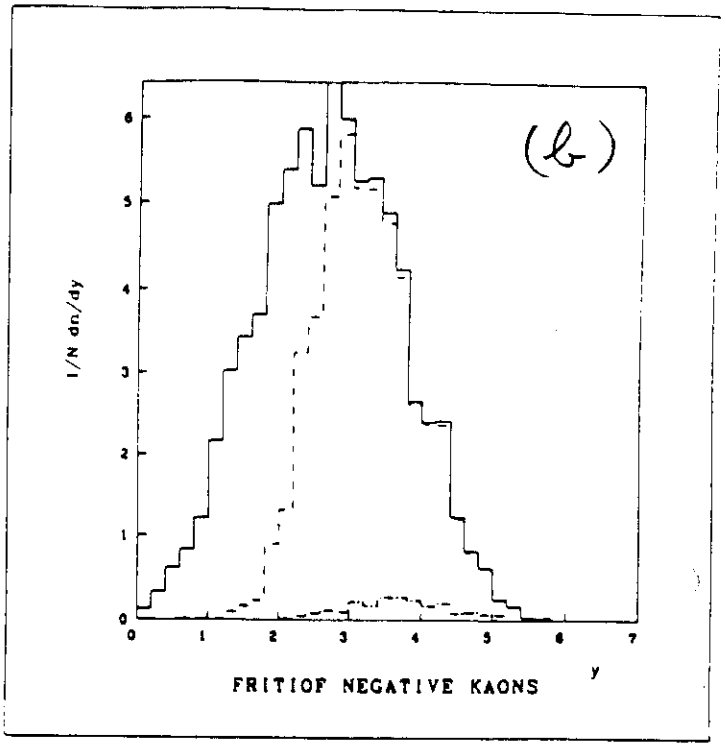
(b)
1/N dn/dy
y
FRITIOF NEGATIVE KAONS

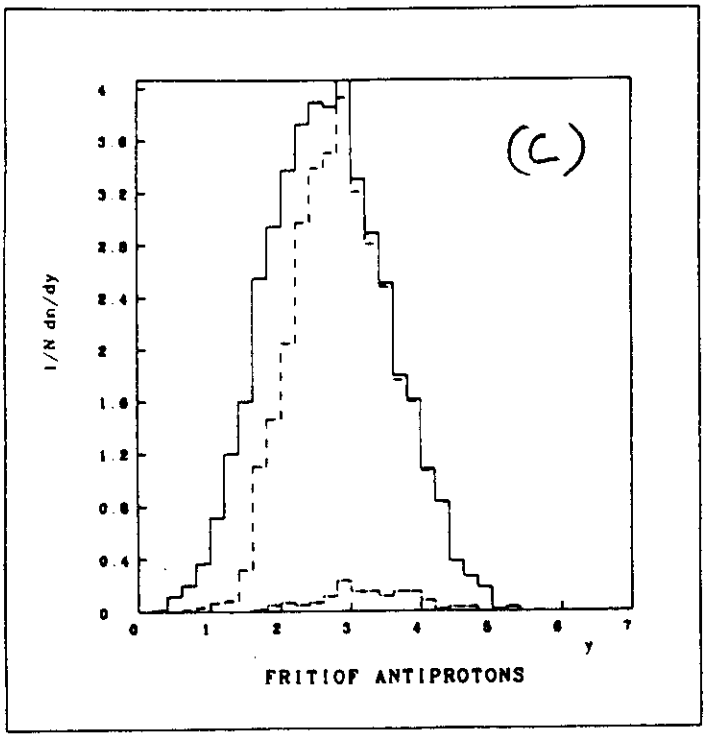
(c)
1/N dn/dy
y
FRITIOF ANTIPROTONS

Fig. 6

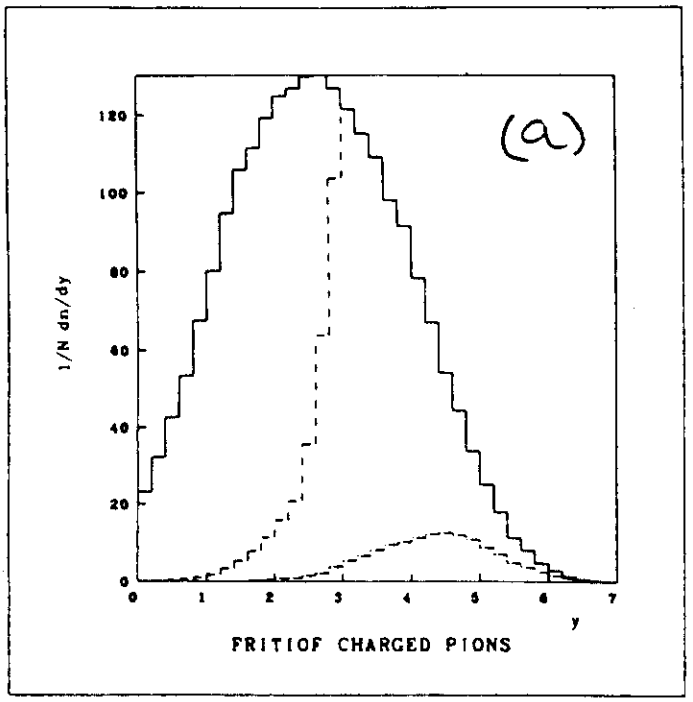
(a)
1/N dn/dy
y
FRITIOF CHARGED PIONS

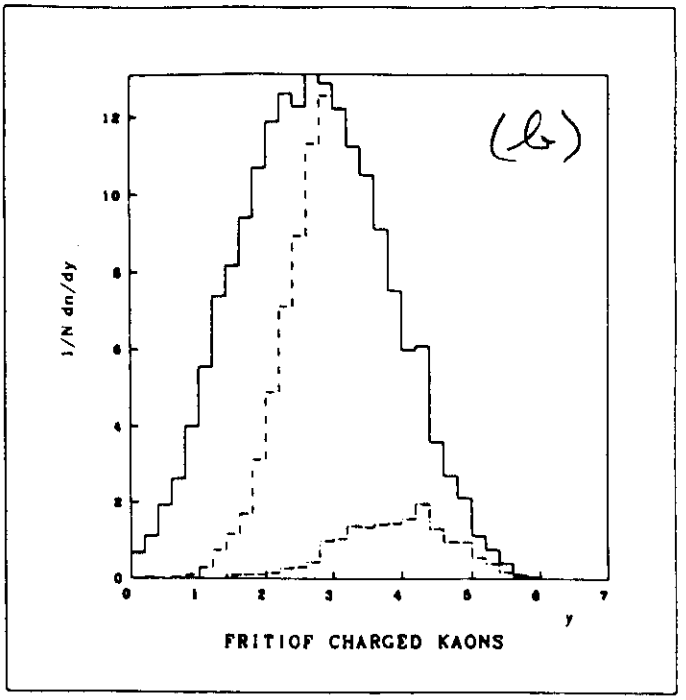
(b)
1/N dn/dy
y
FRITIOF CHARGED KAONS

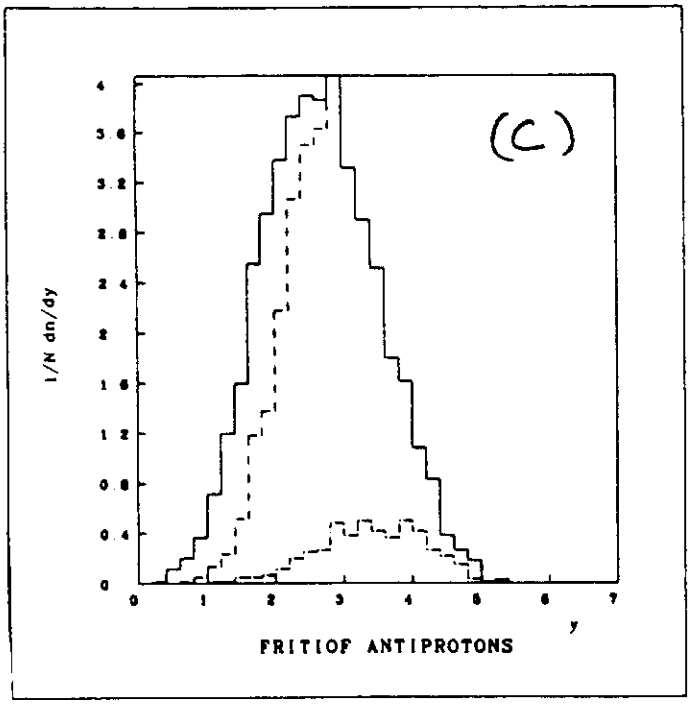
(c)
1/N dn/dy
y
FRITIOF ANTIPROTONS

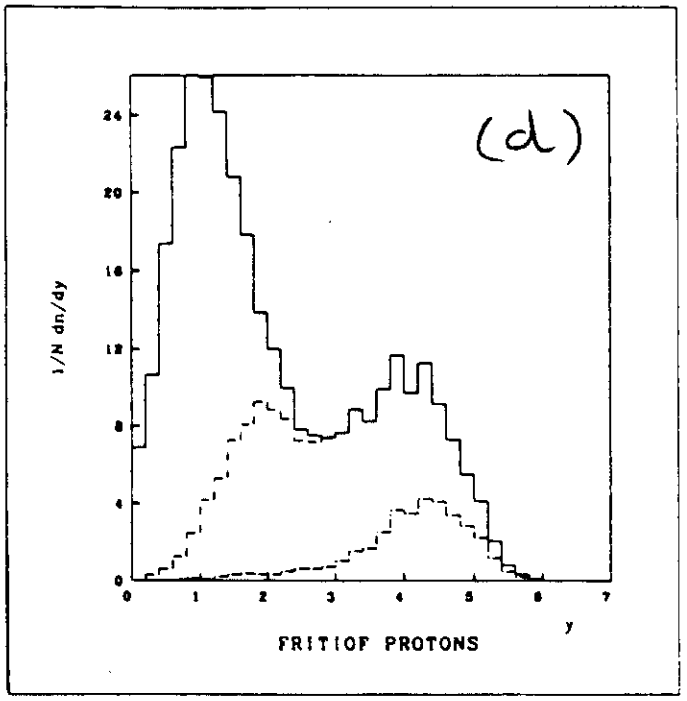
(d)
1/N dn/dy
y
FRITIOF PROTONS

Fig. 7

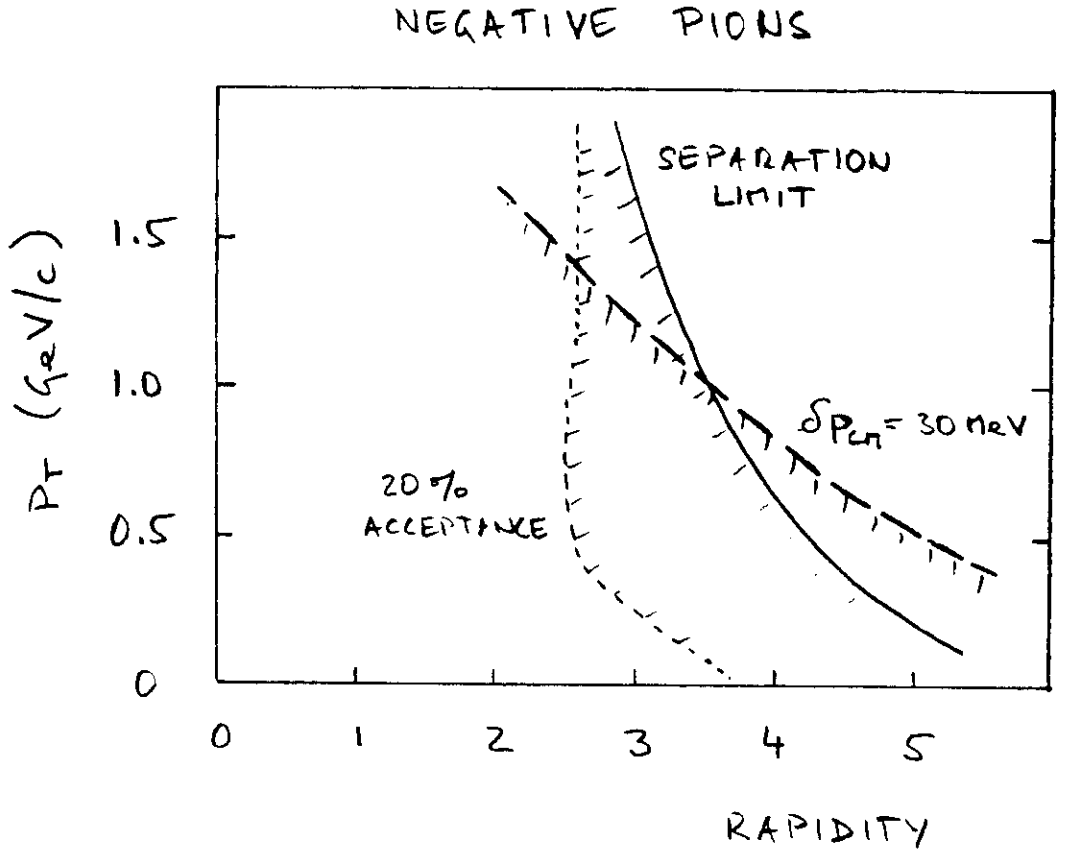
NEGATIVE PIONS
SEPARATION LIMIT
δP_{CM} = 30 MeV
20 %
ACCEPTANCE
P_T (GeV/c)
1.5
1.0
0.5
0
0
1
2
3
4
5
RAPIDITY

Fig. 8

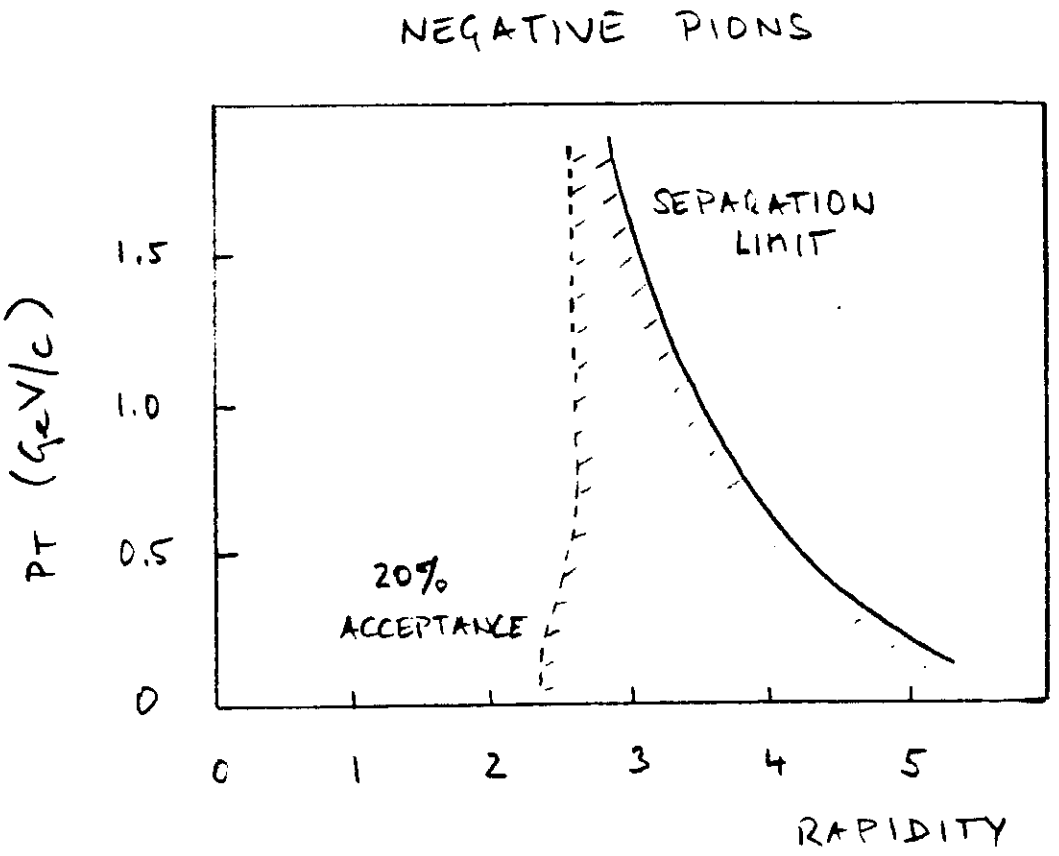
NEGATIVE PIONS
SEPARATION LIMIT
20% ACCEPTANCE
PT (GeV/c)
1.5
1.0
0.5
0
0
1
2
3
4
5
RAPIDITY

Fig. 9

7400 EVENTS , $3.5 < Y_{\pi\pi} < 4.5$

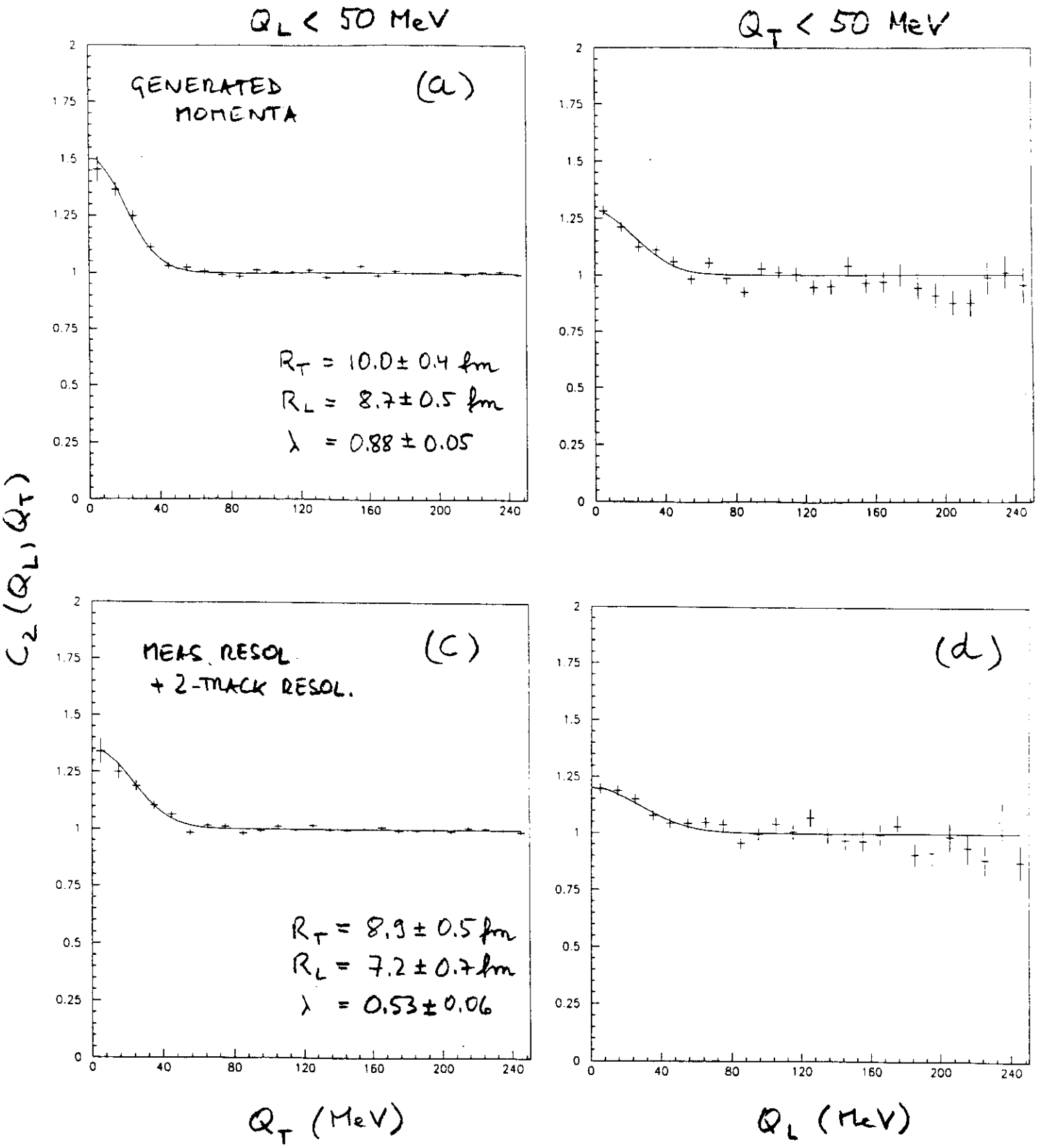

Fig. 10

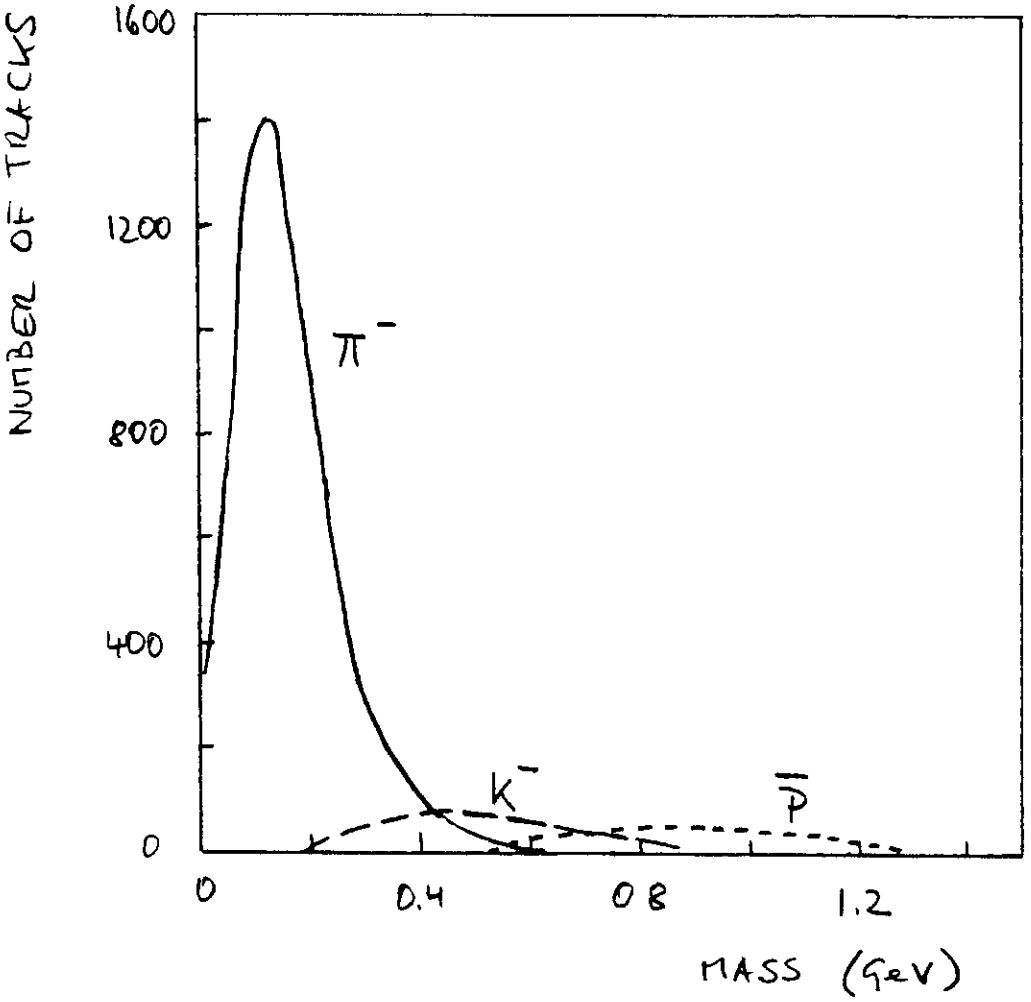
NUMBER OF TRACKS
1600
1200
800
400
0
π^-
K^-
$\bar{p}$
0
0.4
0.8
1.2
MASS (GeV)

Fig. 1i

Fig. 12

PAD PLANE TPC NA 35

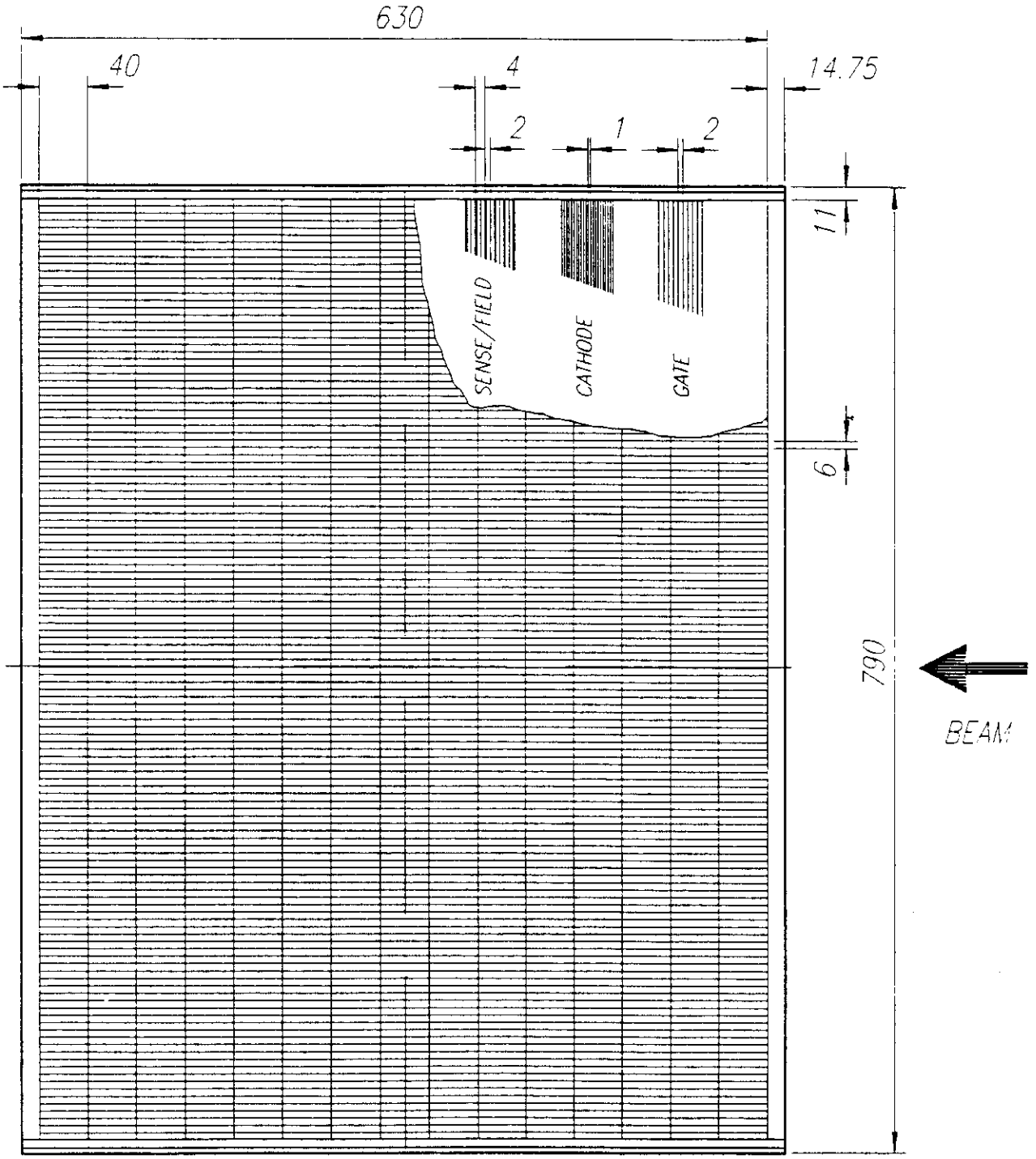

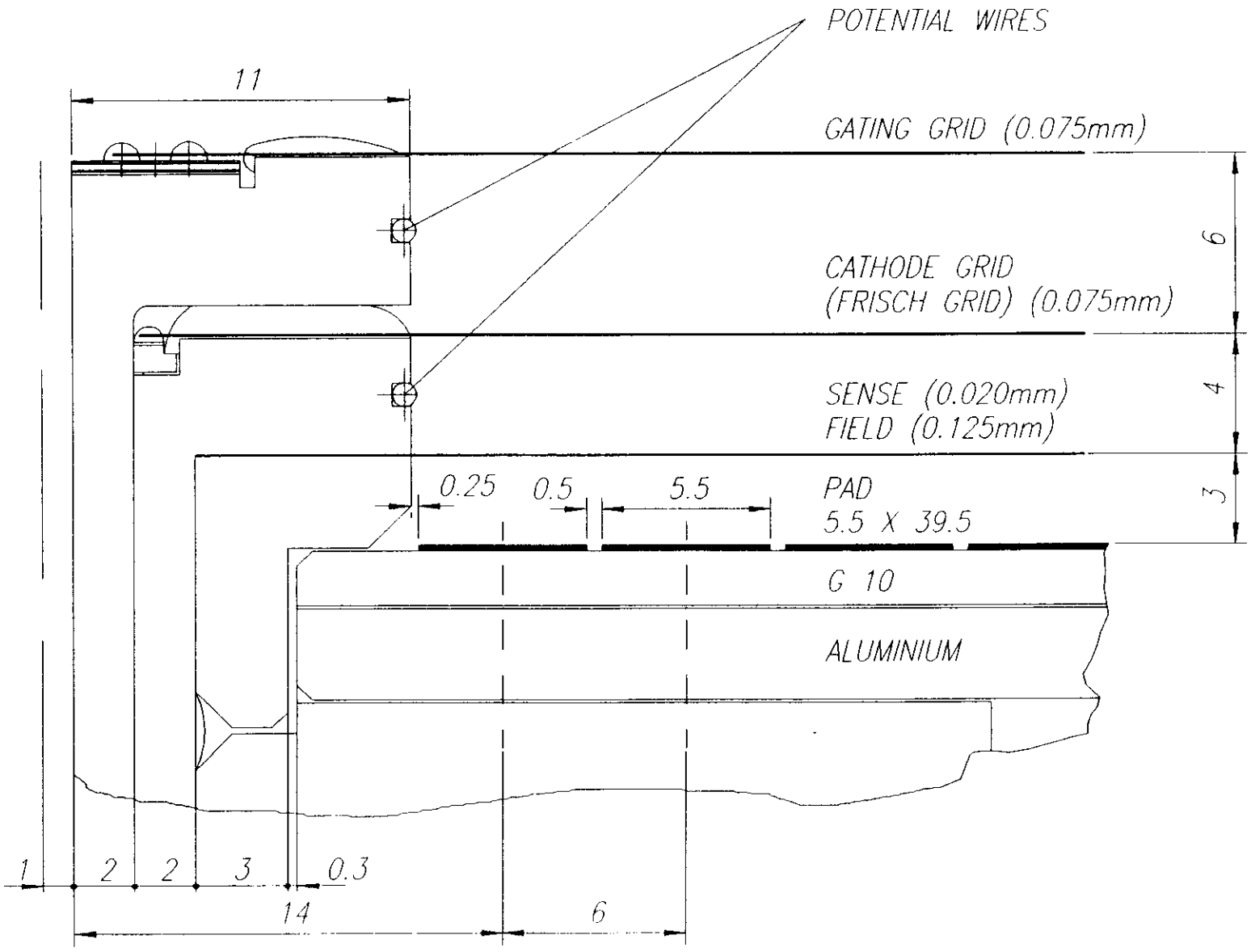
POTENTIAL WIRES
11
GATING GRID (0.075mm)
CATHODE GRID
(FRISCH GRID) (0.075mm)
SENSE (0.020mm)
FIELD (0.125mm)
0.25
0.5
5.5
PAD
5.5 X 39.5
G 10
ALUMINIUM
6
4
3
1
2
2
3
0.3
14
6

Fig. 13

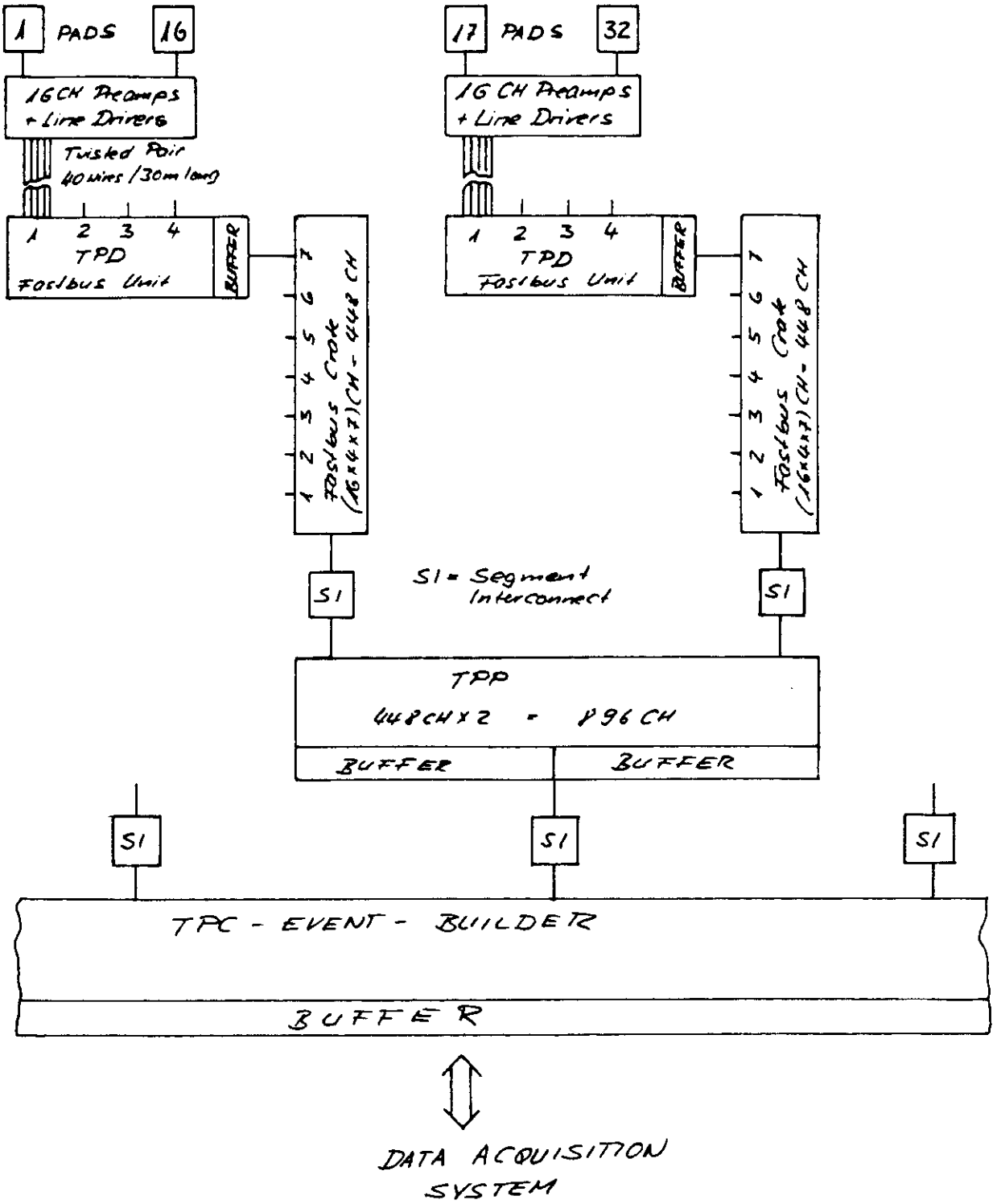

TPD – Time Projection Digitizers
(Line Receivers, Shaping Amplifier, Flash ADC)

TPP – Time Projection Processor

Fig. 14

Equipotential lines for Positive ion effects

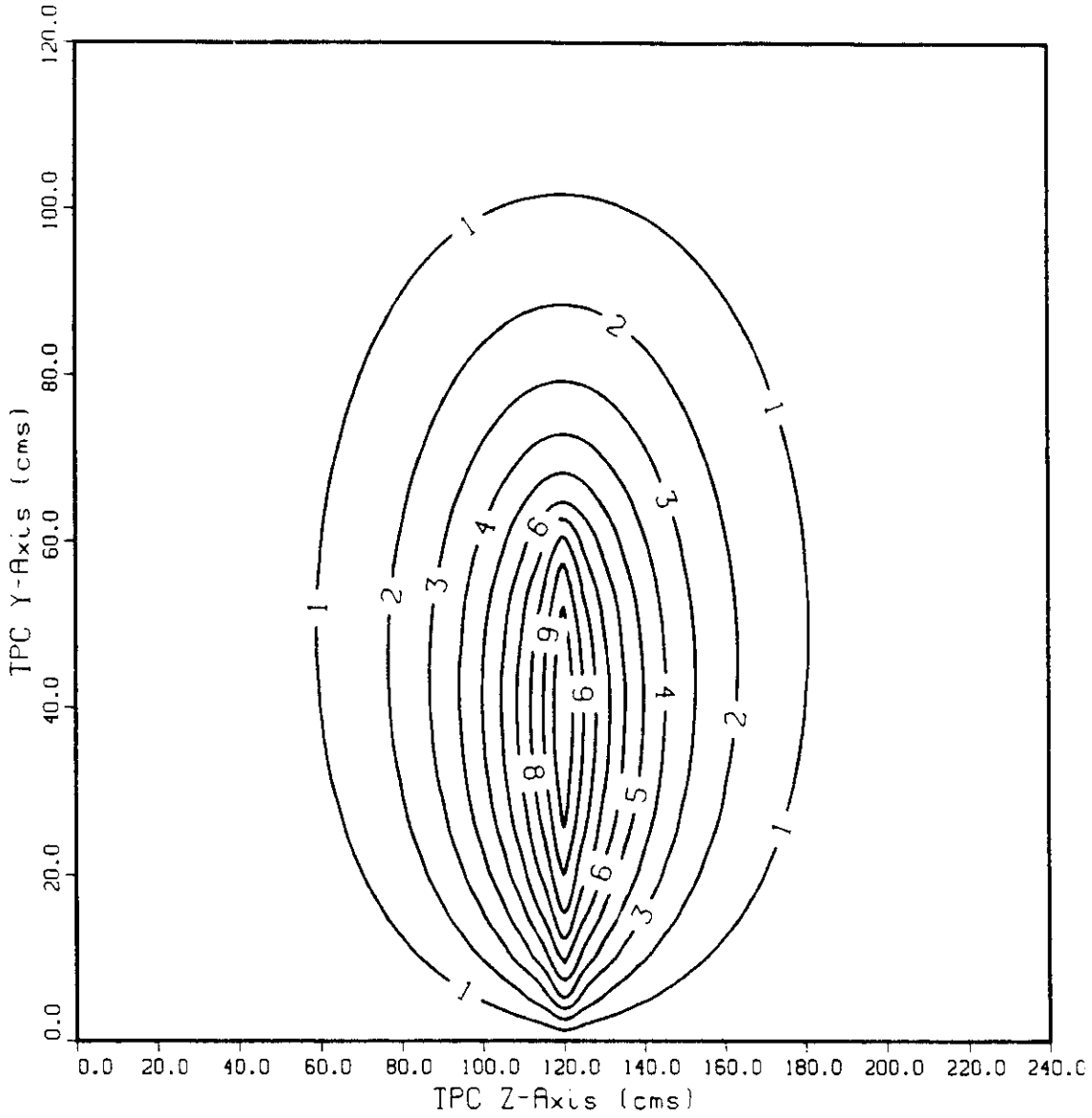

Fig. 15

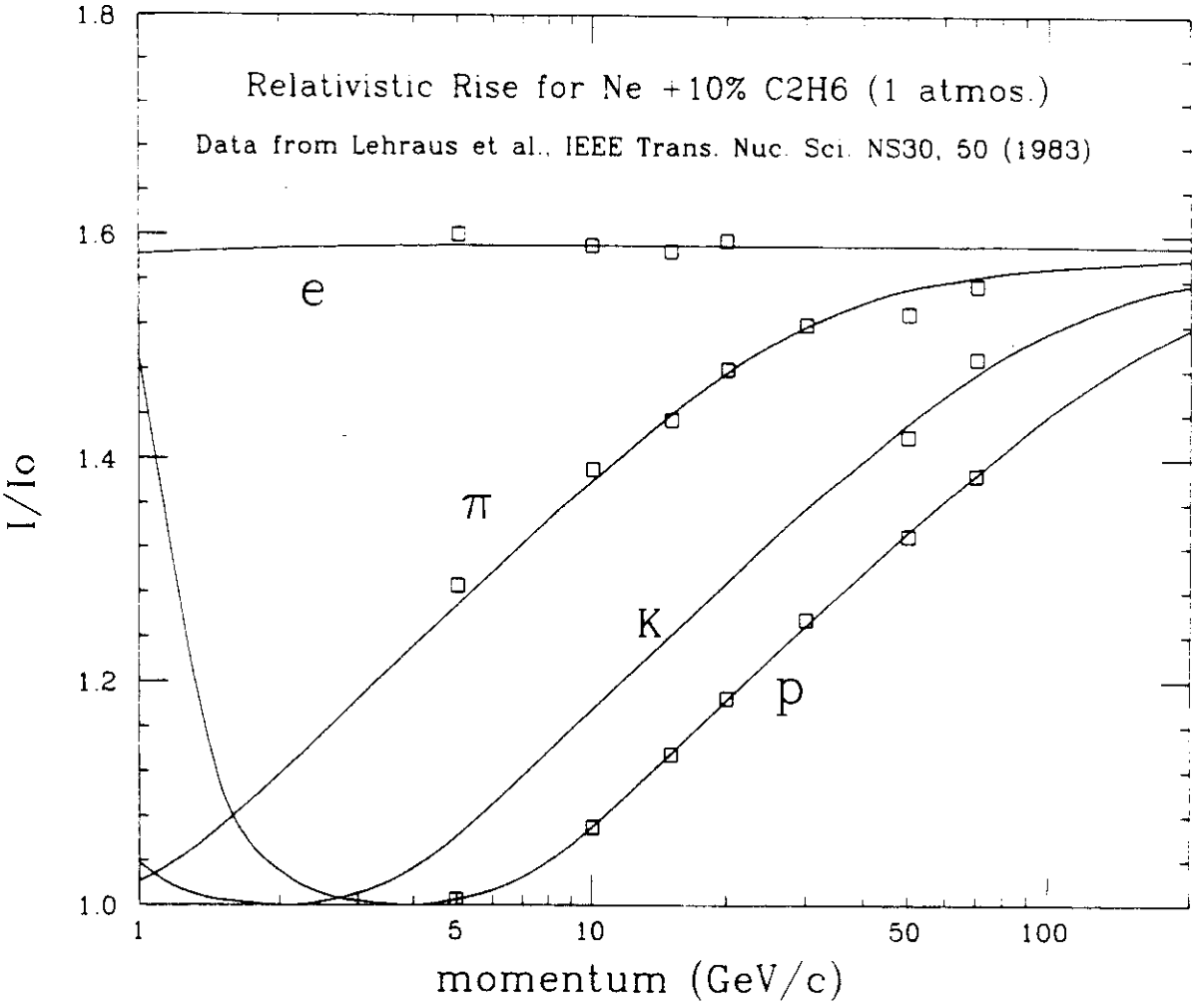
Relativistic Rise for Ne +10% C2H6 (1 atmos.)
Data from Lehraus et al., IEEE Trans. Nuc. Sci. NS30, 50 (1983)
e
π
K
p
I/Io
momentum (GeV/c)
1.8
1.6
1.4
1.2
1.0
1
5
10
50
100

Fig. 16